

Doctoral Dissertation(Shinshu University)

**Oil palm fruit maturity evaluation with inductive coil and
fruit battery method**

**(誘導コイルと果実電池法を用いたオイルパーム成熟度評
価)**

NOR AZIANA BINTI ALITEH

Energy and Systems Engineering Division, Shinshu University

MARCH 2022

ABSTRACT

The purpose of this thesis is to look into two distinct sensor applications for pre- and post-harvest evaluation. A sensor that determines the maturity of oil palm fruit bunches through the use of a triple flat-type inductive sensor concept based on a resonant frequency technique is implemented for preharvest evaluation, which consists of weekly assessments. Post-harvest evaluation employs a fruit battery method that yields immediate results suitable for use at the mill, immediately prior to the extraction process.

Traditionally, an oil palm fresh fruit bunch (FFB) is inspected for ripeness using a human grader, which can be inconsistent and inaccurate. Numerous new methods for grading the ripeness of oil palm FFB have been proposed, and this research aims to propose an alternative to the oil palm maturity detection method by utilizing the coil inductance and fruit battery method. The purpose of this research is to develop a triple flat-type coil inductive-based oil palm fruit maturity sensor with two distinct structure parameters that are either constant in length or in number of turns. The results revealed a relationship between the change in peak resonance frequency and fruitlet capacitance and the moisture content of the fruit sample, which could be used to determine its ripeness stage. The inductive oil palm fruit sensor's sensitivity is increased through analysis of the triple resonant frequencies generated by the triple flat-type air coil structure. The triple series technique, depending on the coil configuration, can increase or decrease the sensitivity of the results obtained in comparison to the single flat-type coil structure. As the fruit ripens, the inductance-frequency curve's peaks move closer to the air's peak curve. Triple coils with the same number of turns but different lengths (Triple I) perform better than triple coils with the same size but different number of turns (Triple II). The development of this sensor demonstrates the inductive element's

capability to be used as a detection element for determining the maturity stages of oil palm FFB during the preharvest stage.

Human vision has traditionally been the primary method for determining the ripeness of postharvest oil palms at the mill. However, relying on human evaluators to grade the ripeness of oil palm FFBs in the traditional manner may result in inaccuracy, resulting in a decrease in the rate of oil palm fruit oil extraction (OER). This study emphasized the fruit battery method for determining the ripeness stage of oil palm fruit FFBs by determining the load resistance voltage and its moisture content resolution. Additionally, computer vision is tested on the same samples using a color feature to compare the accuracy score obtained with a support vector machine (SVM). The fruit battery's accuracy score, computer vision's accuracy score, and a combination of both methods' accuracy scores are evaluated and compared. After testing the ripe and unripe samples for load resistance voltages ranging from 10 Ω to 10 k Ω , three resistance values were selected and tested for moisture content resolution evaluation. A 1 k Ω load resistance demonstrated the highest moisture content resolution, and the results were compared to computer vision accuracy scores. According to the obtained results, the combination method has the highest accuracy, followed by the fruit battery and computer vision methods.

TABLE OF CONTENTS

	Page
ABSTRACT	i
TABLE OF CONTENTS	iii
LIST OF TABLES	v
LIST OF FIGURES	vi
LIST OF ABBREVIATIONS	viii
LIST OF SYMBOLS	ix
CHAPTER	
1 INTRODUCTION	
1.1 Background	1
1.2 Problem statements	3
1.3 Objectives	3
1.4 Thesis contribution	3
1.5 Scope of work and limitation	4
1.6 Thesis outline	4
2 LITERATURE REVIEW	
2.1 Overview	6
2.2 Oil palm fruit	6
2.2.1 Oil palm fruit botany	6
2.2.2 Oil palm fruit chemistry	8
2.2.3 MPOB grading guidelines	12
2.3 Oil palm fruit sensing trends summary	16
2.4 Summary of related research	19
2.3.1 Optical spectroscopy	20
2.3.2 Laser	25
2.3.3 Raman spectroscopy method	26
2.3.4 Thermal	29
2.3.5 Microwave	30
2.3.6 Inductive	31
2.3.7 Capacitive	33
2.3.8 Fruit battery	34
2.3.9 Electronic nose	35

2.3.10	Ultrasonic	36
2.4	Discussion	36
2.5	Summary	38
3	PREHARVEST EVALUATION	
3.1	Overview	39
3.2	Experimental analysis	39
3.2.1	Self-capacitance and fruitlet capacitance	42
3.2.2	Comparison analysis method	44
3.3	Results and discussions	48
3.3.1	Bunch moisture content	48
3.3.2	Inductance-frequency graph characteristics	49
3.3.3	Peak resonance frequency, f_R	49
3.3.4	Fruitlet capacitance, f_R	55
3.4	Summary	60
4	POSTHARVEST EVALUATION	
4.1	Overview	62
4.2	Sample preparation and moisture content determination	62
4.3	Methodology	63
4.3.1	Basic concept of fruit battery method	64
4.3.2	Selecting load resistance value	65
4.3.3	The changing rate of the load resistance voltage	66
4.3.4	Resolution of estimated moisture content	67
4.3.5	Computer vision	67
4.3.6	Accuracy scores	70
4.4	Results and discussions	70
4.4.1	The load resistance voltage differences	70
4.4.2	Resolution of estimated moisture content	72
4.4.3	Comparison evaluation of fruit battery method and computer vision	74
4.5	Summary	78
5	CONCLUSIONS	79
	REFERENCES	82
	APPENDIX	86

LIST OF TABLES

Table		Page
CHAPTER 2		
2.1	Oil palm FFB classification according to Oil Palm Manual by MPOB [4]	12
2.2	Bunch classifications [4]	14
2.3	Summaries of method applied for oil palm FFB quality evaluation mentioned in the order of appearance in this section for spectroscopy method	37
CHAPTER 3		
3.1	Experiment setup parameters for triple flat-type air coil	40
3.2	Type of coil configuration for triple series flat type air coil sensor	41
3.3	Triple series coil mean resonance frequency for ripe and unripe with difference between them	51
3.4	Triple series coil $\alpha\beta$ value for resonance frequency against week and moisture graph	52
3.5	Resonance frequency difference evaluation for triple series air coil	54
3.6	Triple coil mean fruitlet capacitance for ripe and unripe with difference between them	55
3.7	Triple coil $\alpha\beta$ line fit value for fruitlet capacitance against week and moisture graph	57
3.8	Fruitlet capacitance difference evaluation for triple series air coil	60
3.9	Comparison between related research outcomes from previous study	61
CHAPTER 4		
4.1	Oil palm fruit ripeness based on moisture content	63
4.2	Fruit battery experimental parameters	66
4.3	Classification condition setting for SVM	70
4.4	Accuracy score and standard deviation of each feature for fruit battery method	75
4.5	Accuracy score and standard deviation of each feature for computer vision method	75
4.6	Accuracy score and standard deviation of each feature for combination of fruit battery and computer vision method	76
4.7	Maximum accuracy score and standard deviation of each feature	77

LIST OF FIGURES

Figures	Page
CHAPTER 2	
2.1	Anatomy of an oil palm tree [6] 7
2.2	Components of oil palm FFB [7] 8
2.3	Chemical contents of the oil palm fresh fruit bunch (FFB) [7] 9
2.4	Oil palm fruit mesocarp development phase [9] 9
2.5	Morphological, biochemical and histology analysis of oil palm fruit development from 30 to 160 DAP [9] 11
2.6	Oil palm FFB grading flowchart [4] 12
2.7	Oil palm fruitlet exocarp and mesocarp color change from unripe to ripe 13
2.8	Three different oil palm FFB ripeness categories on the same tree 13
2.9	The oil palm fruit ripeness for L_s - f curve for single-flat type air coil for air, ripe, and unripe oil palm fruitlet [44] 32
CHAPTER 3	
3.1	(a) Self-capacitance between coil turns and (b) oil palm fruit ripeness for L_s - f curve for single-flat type air coil for air, ripe and unripe 40
3.2	(a) Experiment setup for triple flat-type air coil sensor and its (b) equivalent circuit 41
3.3	Triple flat-type air coil sensor (a) without and (b) with sample 42
3.4	L_s - f curve illustrates (a) self-resonance frequency (SRF) and (b) resonance frequency 43
3.5	Resonance frequency for (a) direct ripe-unripe comparison, (b) resonance frequency against week and (c) resonance frequency against moisture comparison for selected flat-type air coil peak 47
3.6	The moisture content for fruit sample bunch A, B, C, D and E 49
3.7	(a) Triple I and (b) Triple II L_s - f curves for air, ripe and unripe conditions 50
3.8	Ripe-unripe 1 st , 2 nd and 3 rd peak resonance frequency comparison for Triple I (a)-(c) and Triple II (d)-(f) 51
3.9	Triple I 1 st , 2 nd and 3 rd peak resonance frequency against week (a)-(c) and moisture (d)-(f) 52
3.10	Triple II 1 st , 2 nd and 3 rd peak resonance frequency against week (a)-(c) and moisture (d)-(f) 53
3.11	Triple I and II resonance frequency evaluation comparison for $\Delta\bar{f}_R$, Δf_{R_w} and Δf_{R_m} 54
3.12	Ripe-unripe 1st, 2nd and 3rd fruitlet capacitance comparison for Triple I: (a)-(c) and Triple II: (d)-(f) 56

3.13	Triple I 1 st , 2 nd and 3 rd fruitlet capacitance against week (a)-(c) and moisture content (d)-(f)	57
3.14	Triple II 1 st , 2 nd and 3 rd fruitlet capacitance against week (a)-(c) and moisture (d)-(f)	58
3.15	Triple I and II fruitlet capacitance evaluation comparison for $\Delta\overline{C}_f$, ΔC_{f_w} and ΔC_{f_m}	59
CHAPTER 4		
4.1	The composition of unripe and ripe fruit [37]	63
4.2	(a) Schematic diagram of fruit battery and (b) simple equivalent circuit of the fruit battery	65
4.3	Fruit battery experimental setup	66
4.4	(a) Experimental setup of computer vision and (b) AR marker-based color chart for automatic color correction	68
4.5	The flowchart of extracting color feature procedure	69
4.6	(a) The load resistance voltage of unripe and ripe as a function of load resistance and (b) the changing rate of load resistance voltage between unripe and ripe fruits	71
4.7	The prediction scatter plot between load resistance voltage and moisture content, (a) 10 Ω , (b) 100 Ω and (c) 1 k Ω	73
4.8	The prototype device that estimates oil palm fruit's moisture content using Raspberry Pi 3 Model B	77

LIST OF ABBREVIATIONS

OER	Oil extraction rate
FFB	Fresh fruit bunch
MPOB	Malaysia Palm Oil Board
RGB	Red Green Blue
HSI	Hyperspectral Imaging
MSI	Multispectral Imaging
UV	Ultraviolet
IR	Infrared
LED	Light emitting diode
C&RT	Classification and Regression Tree
NIR	Near infrared
PLS	Partial Least Square
OHW	Optimum harvesting week
SWIR	Shortwave Infrared
Ft-NIR	Fourier Transform near infrared
DOBI	Deterioration of Bleachability Index
FFA	Free fatty acid
OPRID	Oil palm ripeness detector
CMOS	Complementary metal-oxide-semiconductor
KNN	K-nearest neighbor classifier
AC	Alternating current
MOS	Metal-oxide-semiconductor
SRF	Self-resonance frequency
SVM	Support-vector machine
AR	Augmented reality
A/D	Analog-to-digital converter
NDVI	Normalize Difference Vegetation Index
GNDVI	Green Normalize Difference Vegetation Index

LIST OF SYMBOLS

Symbols		Unit
N	Number of turns	
l	Coil core length	(m)
X	Reactance	(Ω)
Z	Impedance	(H)
C_S	Self-capacitance	(F)
C_{air}	Air coil self-capacitance	(F)
C_f	Fruitlet capacitance	(F)
f_R	Resonance frequency	(Hz)
L	Inductance	(H)
C	Capacitance	(H)
f_{SRF}	Self-resonance frequency	(Hz)
L_{max}	Maximum inductance	(H)
w	Coil core width	(m)
h	Coil core height	(m)
$L_{aircoil}$	Inductance of air coil	(H)
L_0	Ideal inductor inductance	(H)
ϵ	Permittivity	(F/m)
ϵ_0	Permittivity of free space	(F/m)
ϵ_r	Relative permittivity of medium	
L_S	Series inductance	(H)
C_R	Self-capacitance at resonance frequency	(F)
$\overline{\Delta f_R}$	Mean resonance frequency difference	(Hz)
$\overline{\Delta f_{Rr}}$	Mean ripe resonance frequency	(Hz)
$\overline{\Delta f_{Ru}}$	Mean unripe resonance frequency	(Hz)
Δf_R	Resonance frequency difference	(Hz)
$\Delta week$	Range of week	(week)
$\Delta moisture$	Range of moisture	(%)
α_{wf_R}	Resonance frequency at Week=0	(Hz)
β_{wf_R}	Sensitivity or gradient of resonance frequency against week	(Hz/week)
α_{mf_R}	Resonance frequency at Moisture=0	(Hz)
β_{mf_R}	Sensitivity or gradient of resonance frequency against moisture	(Hz/%)
$\overline{\Delta C_f}$	Mean fruitlet capacitance difference	(F)
$\overline{\Delta C_{fr}}$	Mean ripe fruitlet capacitance	(F)
$\overline{\Delta C_{fu}}$	Mean unripe fruitlet capacitance	(F)
ΔC_f	Fruitlet capacitance difference	(F)
α_{wC_f}	Fruitlet capacitance at Week=0	(F)
β_{wC_f}	Sensitivity or gradient of fruitlet capacitance against week	(F/week)
α_{mC_f}	Fruitlet capacitance at Moisture=0	(F)

β_{mC_f}	Sensitivity or gradient of fruitlet capacitance against moisture	(F/%)
c_v	Coefficient of variation	
σ	Standard deviation	
σ_c	Standard deviation for resonance frequency	(Hz)
σ_f	Standard deviation for fruitlet capacitance	(F)
$\bar{\Delta}$	Differences mean	
$\bar{\Delta}f_R$	Resonance frequency differences mean	(Hz)
$\bar{\Delta}C_f$	Fruitlet capacitance differences mean	(F)
Nf_{rr}	Normalized resonant frequency of ripe samples	(Hz)
Nf_{ru}	Normalized resonant frequency for unripe samples	(Hz)
Nf_r	Normalized resonant frequency	(Hz)
V_i	Electromotive force	(V)
R_i	Internal resistance	(Ω)
V_L	Load resistance voltage	(V)
d_{VL}	Load resistance voltage differences between unripe and ripe	(V)
V_{LRipe}	Ripe fruit's load resistance voltage	(V)
$V_{LUnripe}$	Unripe fruit's load resistance voltage	(V)
R_{ave}	Average for red color feature	
G_{ave}	Average for green color feature	

CHAPTER 1

INTRODUCTION

1.1 Background

Palm oil has a lot of potential because it is a cheap performing product. Besides its well-known commodity as vegetable oil, it is also used as a biofuel. Its derivatives also have so much potential to be explored and are used in a versatile number of products. Therefore, the demand for oil palm is projected to soar since it has the highest yield of all oil producing crops per acre. It is also the most affordable source of fat for the under-developing regions in Asia and Africa that comprise 82% of the equivalent total global oil palm consumed [1].

Elaeis guineensis is the most common species of oil palm cultivated in Malaysia for commercialization due to its thick mesocarp and thin endocarp [2]. However, Malaysia's average oil extraction rate (OER) has remained stagnant for the past 40 years [1]. The necessity to improve the OER yield without increasing oil palm plantation expansion is detrimental in order to prevent further deforestation while also sustaining the supply and demand. Oil palm OER mainly depends on the oil content of the fruits, the age of the oil palm tree, soil condition, pest, rainfall, harvesting practice, and oil extraction efficiency in the mill. The oil palm fresh fruit bunch (FFB) harvested needs to be processed immediately in its fresh state because the carotene degradation begins immediately after the fruit bunches are harvested [3].

Generally, there are two types of quality inspection: preharvest and postharvest. A preharvest evaluation is conducted by the grader at the plantation to select the ripe bunches. The post-harvesting grading process is evaluated at the mill before the oil palm FFB undergoes

extraction. Oil palm FFB harvested must be delivered to the oil mill within 24 hours in order to avoid its quality deteriorating. Hence, the oil palm mill is located close to the plantations. Oil palm FFB needs to be classified accordingly in order to ensure the high yield of extraction rate per consignment and to prevent it from getting penalized for poor bunch quality [4].

Due to the critical nature of determining the optimal stage of maturity of the selected oil palm FFB prior to harvesting and also postharvest evaluation at the mill, numerous studies on grading the oil palm fruit have been conducted. The standard procedure for grading oil palms is typically accomplished visually by human graders using an oil palm grading manual, such as that used by the Malaysian Palm Oil Board (MPOB). This thesis discusses the pre- and postharvest conditions for the sensors mentioned above, which have varying applications. Pre-harvest conditions include weekly evaluations using an inductive coil method, while post-harvest conditions include immediate determination using the fruit battery method.

1.2 Problem statements

Grading the ripeness stages of oil palm fruits is one of the most widely discussed issues in the oil palm industry. Reliance on human graders to determine the maturity of fresh oil palm fruit bunches has been a traditional method of determining the fruit's ripeness [4]. Nonetheless, human graders are susceptible to errors when determining the ripeness of a fruit based on the color of its skin and the number of loose fruitlets that have fallen to the ground. The primary challenge for researchers is to differentiate the ripeness category of oil palm FFB so that the oil palm mill can maximize the extraction rate and speed up the grading process.

The differentiation evaluation process is divided into two situations: pre and post harvesting for oil palm fruit ripeness grading. The evaluation by the oil palm plantation and the evaluation of the oil palm fruit consignment at the mill to identify good quality bunches and low-quality bunches. The question that arises in this study is how the grading method can be evaluated by using the inductive coil and fruit battery method in two different situations.

1.3 Objectives

The objectives of this research are as follows:

1. To summarize the various methods of oil palm fruit sensing in the literature
2. To investigate the preharvest evaluation of a triple flat type air coil during its ripening stage.
3. To explore the postharvest evaluation using the fruit battery method and compare it with the computer vision method.

1.4 Thesis contributions

This study includes evaluation of the post-harvest and pre-harvest stages using different methods. The preharvest method involves the application of a novel inductive triple-type air coil sensor that was investigated and thoroughly tested weekly. The postharvest methods

introduced in this thesis are the fruit battery and computer vision methods. The fruit battery method is quick but destructive; hence, it is not suitable for the preharvest method as it needs to be processed immediately after testing. The computer vision method, which is non-destructive and commonly used for evaluation, was compared together with the combination method. Preharvest and postharvest evaluations are done in order to understand the process of the grading method.

1.5 Scope of work and limitation

The preharvest flat-type air coil sensor was developed based on the best structure mentioned in the previous study's basic structure and principle [5]. There are two types of triple flat-type series introduced, namely Triple I and Triple II. Triple I has a fixed number of turns N , whereas Triple II has a fixed air core length of l . Due to the limitations of the impedance analyzer, both types require the peak to be within 10 MHz. The samples are tested weekly, and their moisture content is measured. The air coil structure is analyzed with different parameters to determine the sensitivity of the sensor.

The postharvest fruit battery method was introduced and experimented to get the immediate results but due to COVID-19 travel restrictions, there is no new data that can be collected, hence the research work on the available data that was collected before the pandemic.

1.6 Thesis outline

Chapter 1 provides an overview of the research, which includes the following sections: background, problem statement, objective, thesis contribution, scope of work, and limitations.

Chapter 2 describes the oil palm fruit plant and its history. Lessons learned from the chapter include the importance of pre- and post-harvest evaluation in determining the oil palm fruit that is best suited for classification, thus improving the quality of the extracted oil. Then the sensing

trend summary and related research were discussed to better understand the research trend. The related research discussed the various methods used to detect oil palm fruit maturity.

Chapter 3 discusses the preharvest evaluation by using a triple type coil for oil palm fruit maturity sensing. This chapter introduces the sensing method that uses a triple flat-type air coil structure to track weekly ripening progress on the oil palm tree. The basic detection concept and experimental methodology, the outcomes of the study, their relationship to the oil palm fruitlet's moisture content, and a qualitative assessment of its ripening condition are discussed.

Chapter 4 evaluate the postharvest sensing method using fruit battery method. Postharvest evaluation is personalized to the sensing device and the research goals. In order to avoid the accumulation of free fatty acids (FFA), which degrades the quality of the extracted fruit oil, the fruit battery method must be completed immediately. Due to differences in height, lighting, and shadow, harvesters may not consistently judge the ripeness of oil palm FFB across plantations. This chapter discusses sample preparation and determining sample moisture content. In this chapter, the accuracy scores for fruit battery and computer vision are compared. The chapter also includes accuracy scores for combining computer vision and fruit battery methods.

Chapter 4 assessment was related to postharvest sensing using a fruit battery. Postharvest evaluation is sensor and research goal specific. This chapter discusses sample preparation and moisture determination, and compares accuracy scores for fruit batteries and computer vision. A combination of computer vision and fruit battery methods is also included.

Chapter 5 presents conclusion to sum up the findings obtained through this study.

CHAPTER 2

LITERATURE REVIEW

2.1 Overview

This chapter discusses the characteristics and background of the oil palm fruit plant. The chapter also discusses the traditional grading guidelines, emphasizing the importance of pre- and post-harvest evaluation in determining the oil palm fruit that is best suited for classification, thereby increasing the quality of the extracted oil from the consignment. Following that, the sensing trend summary and related research were discussed in order to gain a better understanding of the trend in this research field. The related research included a discussion of the various methods used in oil palm fruit maturity detection.

2.2 Oil palm fruit

Elaeis guineensis, or oil palm tree, is a perennial tropical tree crop grown for its vegetable oil and a potential source for sustainable biodiesel fuel. This section summarized the botany of the oil palm tree in terms of cultivar, classification, and structure. The chemical composition of the oil palm fruit was then discussed. Following that, the Malaysian Palm Oil Board's (MPOB) grading guidelines are examined for clarification.

2.2.1. Oil palm fruit botany

The oil palm tree (*Elaeis guineensis*) comes from *Palmae* family, subfamily *Cocoideae* with genus *Elaeis*. *Elaeis* came from a Greek word, *elaion* means oil. The genus contains two main species: African oil palm (*E. guineensis*) and American oil palm (*E. melanococca*). Figure 2.4 shows the anatomy of an oil palm tree that consist three primary components: tree trunk, frond and fruit bunch.

The oil palm tree (*Elaeis guineensis*) comes from the *Palmae* family, subfamily *Cocoideae*, with the genus *Elaeis*. *Elaeis* came from a Greek word, *elaion*, meaning oil. The genus contains two main species: African oil palm (*E. guineensis*) and American oil palm (*E. melanococca*). Figure 2.4 shows the anatomy of an oil palm tree that consists of three primary components: the tree trunk, frond, and fruit bunch.

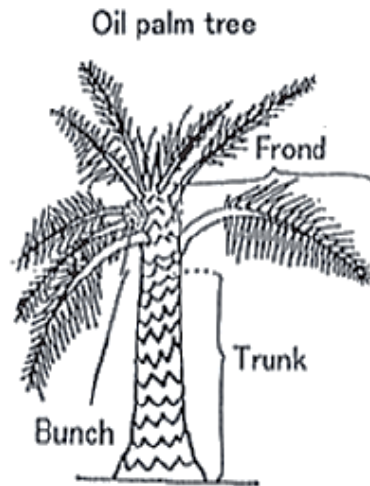


Figure 2.1: Anatomy of an oil palm tree [6]

Each mature oil palm fresh fruit bunch (FFB) contains approximately 1000–4000 individual fruitlets and weighs approximately 15 kg–25 kg. As illustrated in Figure 2.2, each fruitlet is primarily divided into four parts: the exocarp, the mesocarp, the endocarp, and the endosperm. The mesocarp of the fruitlet contains a high concentration of carotenoids, while the kernel oil extracted from the endosperm is yellowish-white in color. Palm oil and palm kernel oil are chemically distinct. In general, oil from the mesocarp accounts for approximately 20% to 22% of the bunch weight, whereas kernel oil accounts for approximately 2% to 3% of the bunch weight. [2].

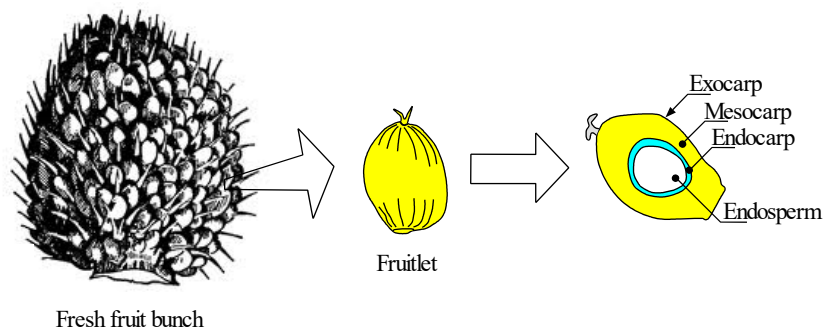


Figure 2.2: Components of oil palm FFB [7]

The classification of oil palm tree cultivars is mainly based on fruit structure and yield. There are four main cultivars: *Dura*, *Macrocaria*, *Pisifera*, and *Tenera*. The *Dura* cultivar has a 2 mm to 8 mm thick endocarp that comprises about 25% to 55% of the fruit weight, with medium mesocarp content by weight of about 35% to 55%. *Macrocaria* is an extreme form of *Dura* with a 6 mm to 8 mm thick endocarp without any commercial value. *Pisifera* has no endocarp with small pea-like kernels with less viable value, but this cultivar is important for commercial crossbreeding palm *Tenera*. *Tenera* is a variety that comes from the hybridization of *Dura* and *Pisifera* with a thinner endocarp (0.5 mm to 3 mm thick) as well as medium to high mesocarp content (60% to 95%), and hence, it is ideal for commercialization [2].

2.2.2. Oil palm fruit chemistry

Elaeis guineensis is a monocotyledonous oil palm. It is a drupe fruit with a lipid-rich fleshy mesocarp tissue that is exceptionally rich in oil, making it the world's highest oil-yielding crop [8]. Figure 2.3 shows the chemical composition of the moisture percentage for ripe and unripe fruitlets. The chemical analysis shows that a ripe fruitlet contains more than 58% lipid (oil) and 24.3% moisture, whereas an unripe fruitlet contains 80% moisture and 5.9% lipid. The residual content of "others" consists of the fruit's fibre component [7].

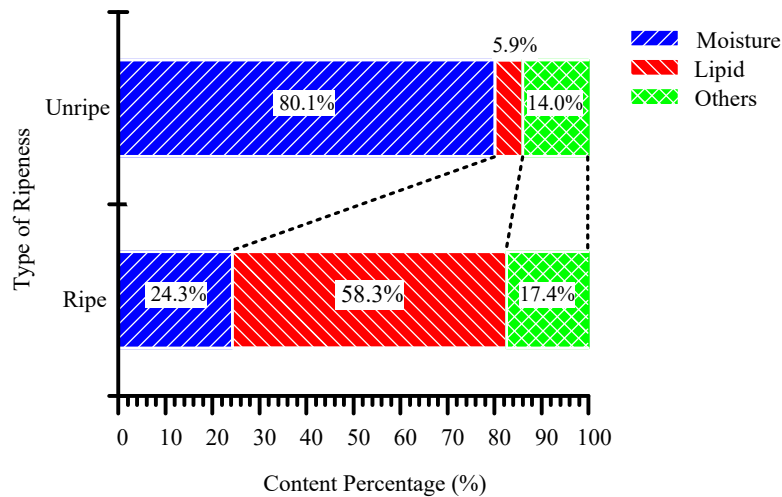


Figure 2.3: Chemical contents of the oil palm fresh fruit bunch (FFB) [7]

The stages of maturity at the time of harvest influence the quality of the fruit. It takes approximately 160 days after pollination (DAP) for the oil palm fruits to complete their development, maturation, and ripening processes. Further analysis of selected histological, biochemical, and hormonal parameters has defined five distinct phases of oil palm fruit mesocarp development, as shown in Figure 2.4. As the fruit ripens, the surface color of the fruit transforms from black to orange, together with its flesh from green to orange due to the presence of carotenoids [9].

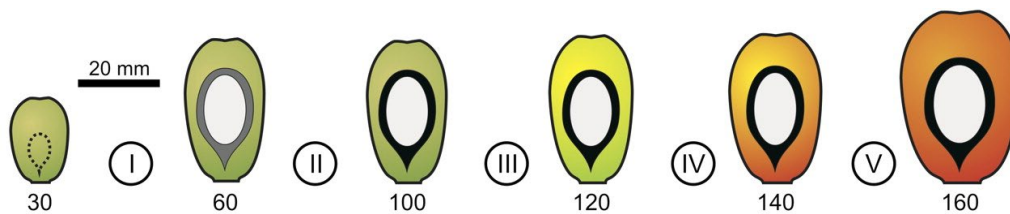


Figure 2.4: Oil palm fruit mesocarp development phase [9]

Phase I is defined by anticlinal cell divisions and expansion along with the initial increase in fruit mass and size as shown in Figure 2.5 (a), (b), (c), and (f). Anticlinal cell divisions are perpendicular to the adjacent layer of cells, which adds thickness to the cell [9]. Phase II, between 60 and 100 DAP, is a transition period characterized by a lag in the accumulation of fresh mass. Phase III, between 100 and 120 DAP, is the end of the transition period. Phase IV

is associated with the beginning of maturation, characterized by an increase in mesocarp fresh mass, the beginning of lipid accumulation characterized by carotenoid accumulation detected by 120 DAP, which is responsible for the colour change from green to orange as in Figure 2.5 (c) and (e). Finally, there is a large increase in the abscisic acid ¹ (ABA) hormones and ethylene during the ripening in phase V, where cell wall detachment related to ripening processes in the mesocarp is visualized in Figure 2.5 (d) and (h). For this phase, dry and fresh fruit mass increase tremendously, alongside with lipid and carotenoid accumulation in the mesocarp that occupy the cell's volume, as in Figure 2.5 (a), (c), (e) and (h). A similar trend was observed with the mesocarp fresh mass, which represents approximately 75% of that of the ripe fruit. In particular, a large increase in dry mass between 120 and 160 DAP reflects lipid accumulation in the tissue as shown in Figure 2.5 (c) and (e) [9].

¹ ABA is the plant hormone involved in stress response.

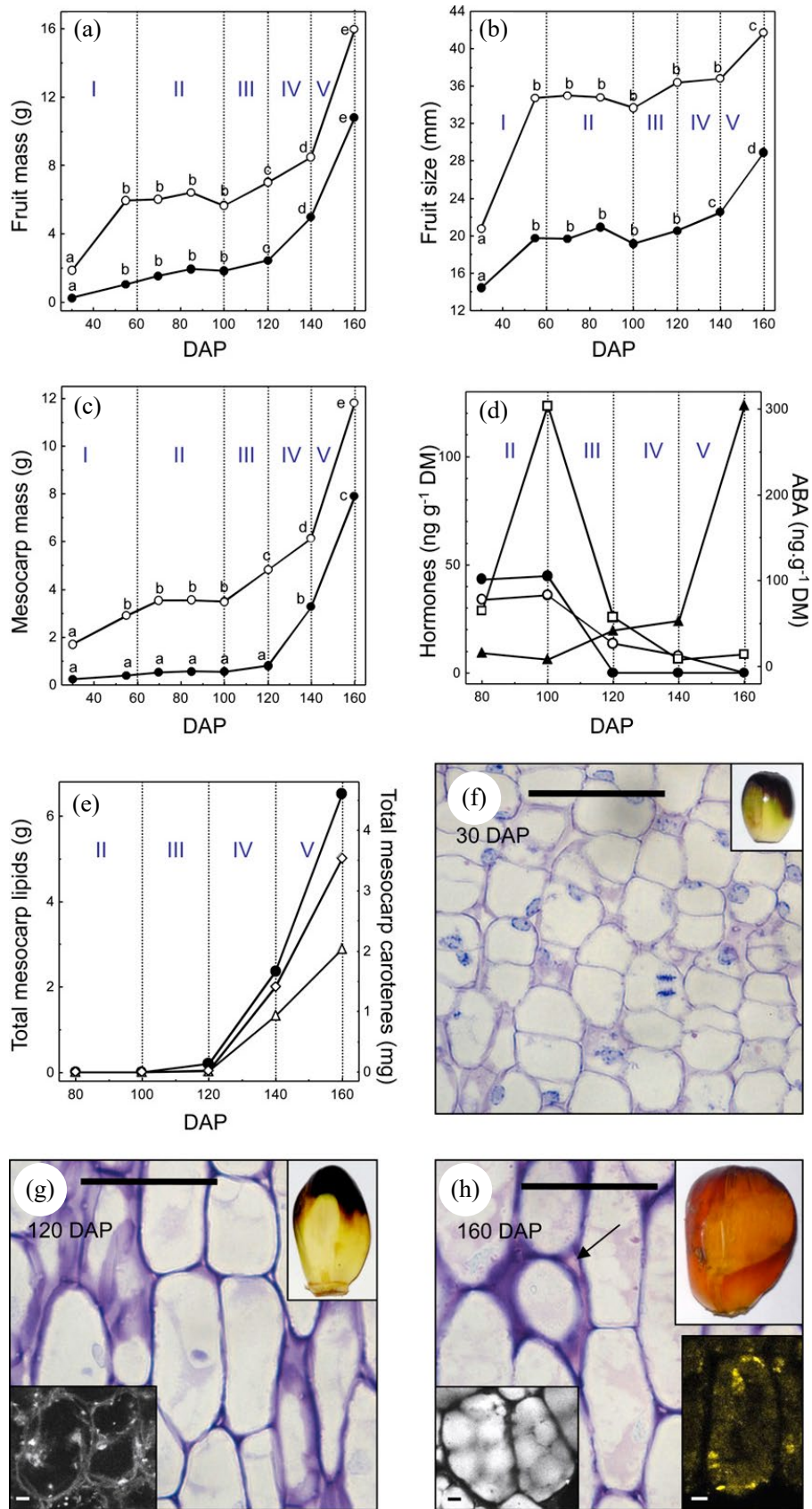


Figure 2.5: Morphological, biochemical and histology analysis of oil palm fruit development from 30 to 160 DAP [9]

2.2.3. MPOB grading guidelines

Quality inspection is classified into two types: preharvest and postharvest. A preharvest evaluation is conducted at the plantation by the grader to identify ripe bunches. The mill's postharvest grading process is evaluated before the oil palm FFB is extracted. The stages of the oil palm FFB grading process at a Malaysian mill are depicted in Figure 2.6. Harvested oil palm FFB must be delivered to the oil mill within 24 hours to avoid degradation in quality. As a result, the palm oil mill is situated near the plantations. Oil palm FFB must be classified appropriately to ensure a high extraction rate per shipment and to avoid being penalized for poor bunch quality [4].

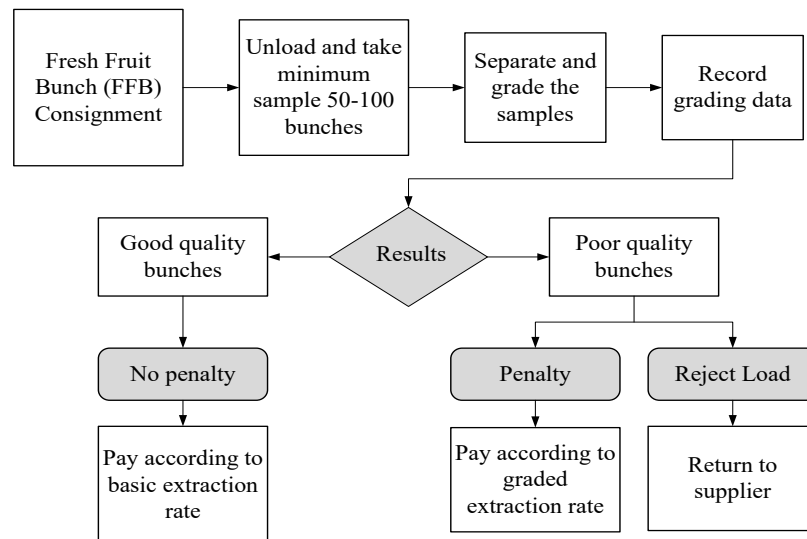


Figure 2.6: Oil palm FFB grading flowchart [4]

Since it is crucial to determine the optimum stage of maturity of the selected oil palm FFB before harvesting and also postharvest evaluation at the mill, various studies were conducted to grade the oil palm fruit. The standard procedure to grade oil palm is commonly done through visual inspection by human graders based on the oil palm grading manual, such as by the Malaysian Palm Oil Board (MPOB). The ripeness of the oil palm FFB is identified primarily by the color of the oil palm fruit exocarp as well as the number of loose fruit or empty sockets in the bunch [4].

The grading process for the oil palm FFB assessment shown in Table 2.1 is based on MPOB standard guidelines that rely on the human grader's decision to evaluate the oil palm FFB based on the number of detached fruitlets and color changes from unripe to ripe as shown in Figure 2.7. Figure 2.8 shows an example of three out of four categories of the fruitlet bunch on one single oil palm tree.

Table 2.1: Oil palm FFB classification according to Oil Palm Manual by MPOB [4]

	Unripe	Under-ripe	Ripe	Over-ripe
Detached loose fruit on the ground (%)	0	10	10-50	50-90
Mesocarp	Yellowish green	Yellowish orange	Orange	Reddish orange
Exocarp	Purplish black	Purplish red	Reddish orange	Dark red

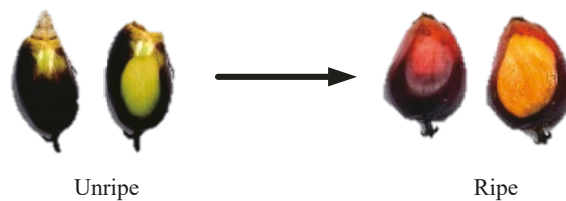


Figure 2.7: Oil palm fruitlet exocarp and mesocarp color change from unripe to ripe

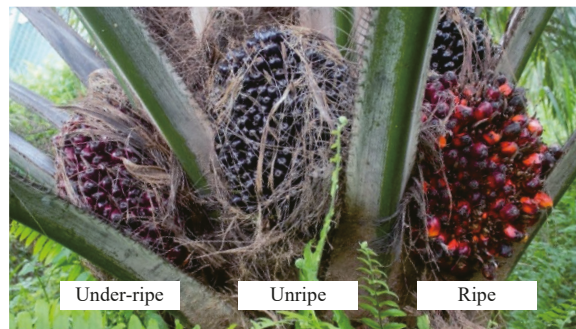


Figure 2.8: Three different oil palm FFB ripeness categories on the same tree

Oil palm FFB need to be classified accordingly in order to ensure that the mill can obtain the maximum extraction rate per consignment. The oil palm FFB can be classified and graded into 15 conditions as summarized in Table 2.2.

Table 2.2: Bunch classifications [4]

No	Bunch classification	Photo	Explanation
1	Ripe		Ripe bunch has reddish orange colour skin and has at least 10 fresh sockets of detached fruitlets with more than 50% of fruit still attached to the bunch during inspection
2	Under-ripe		This bunch is fresh bunch with reddish orange colour and purplish red colour with the outer layer mesocarp being yellowish orange. The bunch has less than 10 fresh sockets of detached fruitlet.
3	Unripe		The fresh bunch has black or purplish black fruit with mesocarp layer being yellowish orange in colour. It does not have any fresh socket of detached fruitlet.
4	Over-ripe		The fresh bunch has darkish red fruit and with 50% detached fruitlet but with at least 10% of the fruit still attached to the bunch.
5	Empty		Bunch with 90% detached fruitlet during the inspection
6	Rotten		Bunch that are partly or wholly turn blackish in colour, rotten and mouldy
7	Long stalk		Long stalk bunch is a fresh bunch which has stalk of more than 5cm in length measured from the lowest level of the bunch stalk
8	Unfresh		Bunch that have been harvested and left on the field for more than 48 hour before sending to the mill. The whole fruit has dried out with dry blackish in colour.
9	Old		Bunch that has been harvested and left in the field before being sent to the field. The fruitlets on the bunch are dry and brownish black in colour with dry, soft fibrous stalk.

Table 2.2: Bunch classifications [4] (cont.)

No	Bunch classification	Photo	Explanation
10	Dirty		Bunch with more than half of its surface covered with dirt or other foreign matters
11	Small		Bunch which has small fruit and weighs less than 2.3kg
12	Pest damaged		Bunch with more than 30% of its fruit damaged by pest such as rat
13	Diseased		Bunch that has more than 50% parthenocarpic ² fruit that are not normal in terms of its size and density
14	<i>Dura</i>		<i>Dura</i> has thick-shell with a thin mesocarp
15	Loose fruit		Fruit that are detached from the bunch due to ripeness with reddish orange colour.

The penalty is based on a discount system imposed on poor quality bunches such as unripe, under-ripe, empty, rotten, long stalk, dirty, *Dura*, and old bunch. Consignment of oil palm FFB with bad quality exceeding 20% and 30% for maximum allowable empty and dirty bunch respectively, will be rejected [4].

The grading process of the oil palm based on the MPOB oil palm fruit grading manual highly relies on human judgement for two ripeness parameters, that is, color change and the percentage of detached fruitlets. The detached loose fruit that indicates the ripening of oil palm FFB from Table 2.1 does not accurately determine its ripeness stage as it does not correlate

² natural or artificially induced fruit production without fertilization ovules

with oil quality and quantity. It has a large variation and is prone to being affected by environmental conditions and human intervention.

The color bias perceived by humans, as well as environmental conditions such as shadow and illumination, can affect parameter grading via change in color of the oil palm FFB. Computer vision makes use of a camera and a computer to mimic the human eye's and brain's image representation capabilities. Machine vision is another term that comes up when it comes to computer vision. Machine vision is a subset of computer vision that consists of machine vision components such as cameras and additional algorithms that can recognize and analyze image data. Color is also affected by the tree's height, and it's only practical for shorter trees because it requires adequate lighting. To eliminate color biases, computer vision was used to aid in the evaluation of the oil palm FFB by human graders.

The origins and motivation for computer vision technology for fruit ripeness identification can be traced back to the fundamental wildlife symbiosis relationship between plants and animals in an ecosystem. Primarily, seed dispersal is one of the crucial aspects of biodiversity conservation of plant species [10]. The dispersion vector includes animal and biotic factors such as wind. In most cases, animals usually facilitate the seed dispersion process, and hence the fruit of the plant exhibits color change and produces an odor when it ripens, which helps to signal it to animals that it is ready to be consumed [11].

During the ripening process, the chlorophyll breaks down and is changed by the antioxidant compounds such as carotenoids and anthocyanins [12]. These compounds change the fruit's color and appearance to prevent it from spoiling rapidly. Likewise, the presence of chlorophyll and carotenoid in the ripening process is one of the main quality factors for grading the oil palm FFB maturity stages. Utom et al. (2018) [13] found that the unripe group has the highest chlorophyll content among all other categories. Chlorophyll is a photoreceptor that has the

capability to absorb light in the visible region with a wavelength of between 400 nm and 700 nm. This is one of the inspirations for the automatic identification of various fruits and vegetables using computer vision technology. Computer vision is widely used to facilitate human food production technology, food safety, and quality control.

Other than computer vision, recent technology has explored a variety of other techniques for evaluating the quality of the fruit using different sensing parameters as the fruit's characteristics change as it ripens. The following section of this paper will delve into more non-computer vision-related topics, as well as combination studies using the non-computer vision method.

2.3 Oil palm fruit sensing trends summary

The journal article was compiled and selected from the last decade of published research on the oil palm fruit sensing method, from 2010 to 2021. The reason for focusing on published research from the last decade is to ensure that the source is credible, relevant, and applicable to current events [14].

Apart from computer vision, researchers in the field of oil palm fruit sensing used spectroscopy, thermal, inductive, capacitive, fruit battery, ultrasonic, electronic nose and microwave sensors. Properties that were investigated include optical, electrical, mechanical, chemical, physical, and thermal.

The keywords used to discover the related papers are "oil palm fruit" with "grading", "ripeness", and "maturity" sensor or detection. The keywords to describe the paper include "quality inspection" and "classification".

The spectroscopy method is most commonly used in food research and industry for various verifications and quality control. This term is primarily defined as the study of interactions between matter and electromagnetic radiation, which allows the structure of matter to be

investigated. The concept of spectroscopy is centered on resonance, where a plot of a type of spectrum that contains peaks is often called a spectral line. However, the term "spectroscopy" is rather broad and not just includes various studies that cover all bands of the electromagnetic spectrum, but also acoustic and particles [15]. Due to its broad range of concepts to various branches of spectroscopy studies, the classification can be divided into two categories: type of radiative energy and nature of interaction.

However, spectroscopy can be classified based on the type of radiative energy and the nature of the interaction. This type of radiative energy categorization includes electromagnetic, acoustic, and particles. The categories based on the nature of interaction are absorption, emission, elastic scattering and reflection, impedance, inelastic scattering, and coherent or resonance spectroscopy. Spectroscopic studies show that the radiant energy interacts with specific types of matter—that can be atoms, molecules, crystals, and so forth. The types of radiative properties include electromagnetic radiation, particles due to its de Broglie waves as a radiative energy source [16], and acoustics that consist of radiated pressure waves and whose visual representation is called a spectrogram [17].

Nonetheless, the most commonly used classification is based on the nature of interaction, as it is more specific to the spectroscopy application that observes the responding properties of the matter being behaving. Examples of interaction are absorption, emission, elastic scattering and reflectance, inelastic scattering and impedance [15]. Spectroscopy basically consists of three imaging instrumentation elements: the radiating source, the subject matter, and the detection array to collect the information.

Optical spectrometry for spectral imaging measures the properties of light that fall under the electromagnetic spectrum and is typically used to analyze and identify materials [18]. Spectral imaging is also known as radiography in the medical field. A camera, commonly used in

computer vision, is an optical instrument that captures images in the human visible band that consists of three colors: red, green, and blue (RGB). Computer vision, as mentioned briefly in the introduction, imitates the basic human vision capability to detect color within the visible region of the electromagnetic spectrum to capture and analyze the object [19].

Hyperspectral imaging (HSI) has the merit of generating chemical maps to show the distribution of parameters [19]. However, HSI poses difficulties in data processing, which are solved by the simplified version of it, namely multispectral imaging (MSI), which consists of fewer bands than HSI. MSI detection work can be focused on selected bands contained in HSI, such as near-infrared, fluorescence, and Raman spectroscopy. Hence, providing flexibility for a range of sensing. Several review papers have been published, the majority of which have focused on computer vision [20], and the purpose of this literature review for this section is to collect and summarize all non-computer vision methods for oil palm fruit ripeness detection applications.

Prior and derivative works were observed in order to discover a new potential detection method other than manual color classification and computer vision that evaluates fruit ripeness using the human visible spectrum. There are a few properties that were tested and explored for the oil palm fruit ripeness grading application, which include optical, physical, chemical, electrical, mechanical, and thermal. All the related research, including research related the sensor proposed in this study, explores the detection possibilities to discover different sensor parameters with the same goal in mind: to distinguish and grade the oil palm fruit.

2.4 Summary of related research

This section is divided into several sections that cover novel research using non-computer vision methods, some of which are computer vision combinations. Spectroscopy is generally an umbrella term generalized for the study related to the interaction between matter and

electromagnetic radiation, which also covers the wide range of the applied electromagnetic spectrum. In this section, studies that conduct a combination of different ranges of electromagnetic radiation spectrum are also included.

The spectroscopy method includes optical spectroscopy, laser light, and Raman spectroscopy. The other methods also mentioned in this section are thermal, microwave, inductive, capacitive, fruit battery, electronic nose, and ultrasonic.

2.3.1. Optical spectroscopy

An optical spectrometer measures the interaction (i.e., absorption, reflection, scattering) of the electromagnetic radiation with the sample, in this case, oil palm fruit FFB. The optical region of the electromagnetic region includes ultraviolet (UV), visible, and infrared (IR) wavelengths. It is worth noting that the optical regions for infrared and ultraviolet contain subregions that divide the spectrum into smaller regions for easy application through wise categorization. For instance, the infrared is broken into near infrared, which is closer to the red in the visible spectrum, and far infrared, which is closer to the microwave and radio region. The UV spectral is divided into three: near ultraviolet, far-ultraviolet, and extreme ultraviolet.

Hazir et al. (2012) [21,22] proposed a multi-parameter fluorescence sensor to investigate the potential of phenolic compounds, specifically flavonoids and anthocyanins parameters, as a predictor to classify the degree of oil palm FFB ripeness. The study from [22] uses 180 oil palm FFB samples for this experiment. Each sample was randomly scanned using a hand-held Multiplex 3 multi-parameter fluorescence sensor. The results showed that the flavonoid and anthocyanin content decreased from unripe to overripe oil palm FFBs. This research proves that flavonoids and anthocyanins can be used as one of the feature indicators for palm maturity classification. For the study in [21], 210 oil palm FFBs with 70 bunches from the underripe, ripe, and overripe categories were used. Each bunch was scanned using the same handheld

Multiplex 3 multi-parameter fluorescence sensor from [22]. The contribution of this study is that the FFB maturity of the oil palm FFB can be estimated using the Blue-to-Red Fluorescence ratio index. The index uses blue-green (447 nm) and far-red (685 nm) ultraviolet light-emitting diodes (LEDs) as excitation light sources. 150 samples were used to develop the training model using the Classification and Regression Tree (C&RT) method that shows the best results with 90% classification accuracy.

Cherie et al. (2015a) [23] tested oil palm FFB optical characteristics under three spectrum regions for harvest decision application. The oil palm FFB were inspected by an expert panelist before being cleaned and transported to a low-temperature dark imaging room. The low temperature aims to delay the degradation of the fruit's lipids after harvesting. For the experiment, UV lamps, which emit light spectrum wavelengths of 320–380 nm, and a halogen lamp that emits electromagnetic spectrum in the visible light region (400–700 nm) and infrared (720–1100 nm), are used for the experiment. UV light is used to evaluate the optical response of FFB through the surface of reflected light. Halogen lamps are used to observe visible light and the IR spectrum. Chlorophyll and carotene pigment have different reactions when illuminated under these lights and due to their pigment light absorption criteria. After the image is captured under different lights, the FFB samples undergo chemical analysis to extract the oil using a Soxhlet extractor. The optical properties of the FFB are identified from the information from the image recorded. The image was then analyzed and converted into a histogram. The linear regression coefficient from samples was correlated to the sample's oil content and grouped according to the spectrum used during the analysis. The optical feature selected for comparison is from the image's histogram, averaged of RGB mean values for red (R_mean), blue (B_mean) and green (G_mean). The results show that the harvested FFB decision can be determined with the image of the sample that has a G_mean value lower than 109.006 or 69.292 when it is recorded at 7 meters under ultraviolet and visible light, respectively.

Another paper by Cherie et al. (2015b) [24] uses the advanced model for camera vision for non-destructive evaluation. This paper study is about the correlation between oil palm FFB appearance and its oil content. The samples were recorded at different distances from the source of light. Similar to [23], the light source used consists of ultraviolet, visible light, and infrared. The FFB images are recorded using a photo selective filter that only passes the selected wavelength of light to the camera. From 20 experiments conducted, only 5 models were valid. The five models are the results of the ultraviolet, visible light, and infrared light at different distances. In this study, it was found that the model developed and labelled as the Vis1-7m arrangement, which records the FFB image under visible light with 600-watt lamps from a distance of 7 meters, shows the best performance among all the setups tested.

Albakri et al. (2018) [25] did an assessment of oil palm FFB maturity based on the diffused reflectance spectroscopy technique by observing the revolution of the specular reflectance spectrum. The reflectance data shows that unripe FFB displays low reflectance compared to higher ripeness bunches. The reflectance characteristics can be related to the change of color due to chlorophyll and carotene concentration ratio. As the FFB ripens, the color of the FFB becomes darker, thus giving higher reflectance values within the visible range of its surface. This method uses the value of spectral reflectance analysis to measure the ratio of chlorophyll to carotenoids. The light sources used for this experiment are ultraviolet and visible light sources. There are two wavelength peaks observed at about 580 nm and 680 nm, which are due to the presence of carotenoid and chlorophyll that produce high reflectance intensity. Ripe and overripe have two major peaks, but the unripe fruit only shows one major peak since the unripe fruit has a low reflectance value. This information can be used to estimate the maturity level of the fruit based on the reflective spectroscopy technique.

Setiawan et al. (2019) [26] also studied using contrast and skewness from a single wavelength of 680 nm image to estimate the oil palm fruit ripeness stages. By using a specific wavelength and a simple image processing technique, they can correlate it with the chlorophyll absorbance wavelength. A total of 101 oil palm FFBs were used in the study, which consists of 24 training and 77 testing datasets. Previous research that utilized LiDAR shows that the reflectance intensity can be used to classify the oil palm ripeness maturity. This research proposes a simple technique that uses an LED with a specific wavelength of 680 nm as the light source and a digital camera. The research uses the contrast and skewness values to estimate the maturity stages of the oil palm FFB. The accuracy of the skewness is chosen to estimate the oil palm FFB maturity as it is the same as the contrast-skewness combination with 68.83% accuracy. This paper proposed a simple system for oil palm grading with low computation to process the image that can be easily applied using a microcomputer.

Iqbal et al. (2019) [27] aim to investigate the feasibility of near-infrared (NIR) spectroscopy to predict water and oil content in FFB by developing a calibration model. 60 FFB samples were tested with the NIRFlex N-500 spectrometer, and their water and oil content were measured. To develop a calibration model, partial Least Square (PLS) regression and preprocessing were conducted, and the results showed that PLS performs well to establish a calibration model to predict water content but poorly for oil content. In a laboratory setting, the model could predict the water content of FFB, but it was limited to samples taken from the same variety and plantation.

Cherie et al. (2019) [28] investigated regarding the determination of the optimum harvest window (OHW) and quality attributes by using shortwave IR spectroscopy. The study proposed using the reflectance shortwave infrared (SWIR) for the optimum harvest window evaluation with its standard attributes. The experiment involved 150 FFBs for 5 different maturity stages,

and its standard quality attributes were correlated with the SWIR data. 100 data points were used as calibration and 50 data points for the validation model. An Ft-NIR spectrometer was used to measure the diffused reflectance of the fruit. The fruit was rotated to have all surfaces recorded and the measurements were repeated using different sets of samples. From naked eye observation, the physical characteristics such as color, shape, and dimension were visually similar for unripe and ripe FFB. The OER, DOBI and carotene value were influenced by the FFB development stage, whereas the FFA value increased when the FFB was over matured as the degradation process began at this time. The quality and price of the oil palm FFB depends on the FFA in palm oil. The maximum FFA content set by the Indonesian Palm Oil Association in crude palm oil is 5%. A high FFA value means it has poor quality oil extracted. Principal Component Analysis (PCA) was used to model the FFB ripeness for evaluation using SWIR spectroscopy. The study was able to develop a SWIR diffused reflectance-based PLS regression model for FFA, DOBI, and carotene. The model validation was performed to confirm the process and activities intended to verify the model.

Prediction using an optical spectrometer by Tuerxun et al. (2020) [29] is a study related to data mining for oil palm maturity classification. A total of 106 oil palm FFB samples with different maturity levels were prepared and divided into 4 categories: unripe, underripe, ripe, and overripe. For this study, the samples were scanned using an OPRID (Oil Palm Ripeness Detector) that uses inbuilt transmission light and a receptor to catch the reflected light. The OPRID used is a portable spectrometer that measures the reflected energy from the surface of FFB in ultraviolet, visible light, and infrared. It has eight different light wavelengths. Four sensors with eight-band wavelength measurement capabilities were installed to detect the reflected light emitted from the eight different LED modules: The sensors detect the reflected wavelength bands at 365 nm, 460 nm, 523 nm, 590 nm, 623 nm, 660 nm, 735 nm, and 850 nm. The sensor detects the amount of energy reflected from the outer surface layer of the oil palm

across the various bands of spectrum mentioned. The classified model provides an accurate classification that can generate a prediction of the oil palm fruit FFB predictive model using light reflectance attributes measured by the OPRID device. The simple lazy KStar algorithm validation performs better, with a 63% classifier model performance.

2.3.2. *Laser*

Laser light has recently been used in agriculture due to its non-destructive nature, which allows for non-invasive experiments to evaluate qualitative parameters of the oil palm fruit. Laser light is an optical technique that measures the interaction of monochromatic light (laser) with the fruit.

Salambue et al. (2018) [30] investigated the ripeness of oil palm FFB using biospeckle imaging, which is based on a laser diode and a CMOS camera. The biospeckle phenomenon occurs when organic matter is illuminated with laser light and the data obtained is optically recorded and produces speckles in light and dark granules. As the fruit ripens, the molecular structure of the fruit tissue will undergo changes that will also affect the optical property of the fruit as the speckle pattern dynamic will also change since the ability of the fruit's skin to absorb and scatter light changes as the fruit ripens. A diode laser, a CMOS camera, biconcave lenses, and image and data processing software were used in this study. The FFBs are chosen from three maturity stages: unripe, ripe, and overripe. The image of the FFB undergoing speckle was captured using a monochrome CMOS camera with a 650 nm laser diode. The biconcave lens used for this purpose focuses on 2–5 pieces of the fruitlets, as illuminating the entire FFB will produce dark dominant speckles. The experiment was conducted in a black box in order to eliminate outside light interference during the measurement. The highest classification results were produced by the front surface of the base section, as the front fruit surface had the most

fruit similarities of all the parts due to its higher scattering intensity due to a more homogeneous scattering surface than any other surface tested.

Another research that uses laser for oil palm fruit grading sensor application is by Mohd Ali et al. (2020) [31]. This paper reports research on optical imaging that uses a laser diode as a light source for food monitoring systems. It uses backscattering imaging and interaction to monitor the quality attributes of agricultural products. This technique was claimed to be cheaper and faster than other optical imaging methods as it does not need correction analysis. This study compares and proposes the combination method of optical imaging using laser diodes with computer vision. There are three oil palm fruit ripeness categories, and the total oil palm FFB tested was 90, with 30 fruits for each category. This study also measures the oil content of the samples with the Soxhlet method on a wet basis at each maturity stage of the sample. The color value was also measured using a colorimeter to get the color data of the fruit. The laser diode used for this study is 658 nm. Fluorescent light is used to illuminate the sample on the platform for the laser light backscattering imaging system. The combined technique of laser backscattering and computer vision for this study shows a good coefficient of determination of more than 0.80 for oil content and color values. The average classification accuracy recorded was also more than 85%.

2.3.3. Raman spectroscopy

Raman spectroscopy is known to detect the molecular vibration of elements, such as carotenoids, that are commonly found on fruit skin. The Raman-based device uses light intensity to measure the inelastic scattering of the targeted compound's surface, with the identified peak known as its molecular fingerprint. Raman spectroscopy is the study of the molecules' vibrational characteristics when a laser light source is used to illuminate the sample [32].

Dan et al. (2018) [32] also tested the oil palm fruit classification using Raman spectroscopy since different characteristics of the Raman shift were detected, which represents the material composition for each sample. The fruit was sliced and prepared by cutting the skin for spectroscopy screening. The samples consist of unripe, ripe, overripe, and rotten fruit. The laser is controlled to avoid thermal decomposition of carotenoid and other organic compounds. Structural damage such as bruises can alter the value of the Raman shift and hence the need to be careful. The ripe spectra show the highest Raman intensity compared to all other ripeness stages compared. After the ripe, other overripe and rotten stages show an increasing trend as the internal compound declines as it passes the ripe stage due to the disintegration of the carotene as it becomes rotten. Raman is suitable to observe changes in organic composition. Raman can differentiate all the vibrational modes related to the key compound to distinguish and monitor the ripening stage of the oil palm fruit. It is found that the carotenoid is the dominant organic composition in the Raman spectrum for the oil palm fruit quality attributes evaluation.

Nokkaew (2019) [33] compares Raman and Fourier transform near-infrared (Ft-NIR) spectroscopy to find the best method to determine the carotenoid and Deterioration of Bleachability Index (DOBI) content. The results indicated that Raman is better for determination than FT-NIR spectrometry. This study aims to compare and determine the qualitative evaluation of the oil palm fruit in crude palm oil. The bunch was separated into 3 zones and divided into ripe and underripe from the same bunch. DOBI and carotenoid content: the DOBI value increases to its maximum at 3 days of storage and then decreases due to the autoxidation over longer storage.

Raj et al. (2021) [34] use Raman spectra to classify the oil palm FFB based on the carotene content. The experiment involves 3 ripeness categories, namely underripe, ripe, and overripe,

with 46 oil palm fruit samples. This study also tests 19 classification techniques to find the classification technique that works best to classify the data from the data obtained. The study found out that the Raman peak averaged at 1515 cm^{-1} , which is known as the molecular fingerprint for the carotene, which is present in oil palm fruit as it ripens. Further analysis of the Raman peak also reveals another four significant sub bands that originate from the carbon double bond (C=C) stretching vibration of carotenoid on the oil palm fruitlet skin. The K-nearest neighbor classifier (KNN) classifier was found to be the one producing the best overall classification with 100% accuracy. The main hurdle posed in evaluating the Raman spectrum is that it consists of a convoluted signal that is made up of different organic compounds. Deconvoluting the spectrum can further synthesize the signal for more accurate classification. The samples used for this study consist of 46 samples, with 14 underripe, 20 ripe, and 12 overripe samples. The target molecular assignments, such as carotene and xanthophyll, consist of pigment colors that contribute to the ripening of the fruit. The deconvoluted bands further expose the details of the carotenoid detected for the quality evaluation of the oil palm fruit can be done effectively on a molecular scale. The study also discovered that beta-carotene is the most abundant carotenoid found in oil palm fruit, and an increase in beta-carotene indicates that the fruit is ripening; the intensity of orange pigment corresponds to the increase in beta-carotene peak. However, the concentration of beta-carotene decreases as it goes overripe. Lycopene is the red color pigment, and an increase in lycopene will cause a red color to be visible on the fruit's skin. This correlates to the finding that the red value in RGB is the highest when it is in ripe stages [35]. This technique is also durable against the effects of noise caused by moisture and illumination.

2.3.4. Thermal

Zolfagharnassab et al. (2016) [36] conducted a study in which they used thermal vision to detect changes in the mean temperature as the oil palm FFB ripens. The prototype thermal device in this study was also compared with the commercial thermal camera for this application. Thermal remote sensing is differentiated with optical remote sensing where the radiation emitted from the surface of the object is measured instead of measuring the radiations reflected by the object. The prototype thermal device produces lower mean temperature compare to the commercial thermal camera with an average of 1.39°C, 1.80°C, and 0.05°C for underripe, ripe and overripe FFBs respectively. The study shows correlation of mean temperature recorded by the prototype and commercial thermal device is significantly correlated with $P < 0.01$ for each category.

Makky et al. (2020) [37,38] initially studied the optical properties of the oil palm FFB [20] and are now exploring thermal imaging methods to identify the optimum harvest window prediction for oil palm fruit. This non-destructive method uses a thermal camera to measure the oil palm FFB skin or surface temperature. The author mentioned that the previous optical system poses limitations as the variation in light intensity greatly influences the color captured by the camera [38]. This method was proposed based on the knowledge that as the fruit ripens, the chemical composition and enzymic reaction will cause a distinct change in the fruit's temperature [38]. For study conducted in [38], a hybrid-camera was used to investigate the changes in oil palm FFB physical and thermal characteristics as they ripen. This approach shows better prediction for FFB compared to the previous study [37]. his study also includes various indicators tested, such as moisture content, oil content, DOBI, carotene, and the ratio of oil and moisture. The FFB ripeness was modelled according to its surface temperature and green spectrum to establish the optimum harvest window, except for the DOBI parameter that is best performed by employing the bluish spectrum of FFB.

2.3.5. Microwave

Microwaves are known to be sensitive to water due to the polarization of the water molecule, as it is known to absorb microwave energy [39]. The change of moisture content using this method can be observed by observing the change in reflection or its coefficient and the change of resonance frequency due to the change in dielectric permittivity. Dielectric properties are highly dependent on the ionic conductivity of fluid in their cellular structure in the fruit. Nevertheless, it is worth noting that the overall structure of water in oil palm mesocarp is complex and should be treated with caution.

You et al. (2020) [39] wrote the review article focusing on the research and measurements of microwave sensors for oil palm fruit ripeness processing applications. A microwave sensor is a device that operates in the microwave frequency range (300 MHz to 300 GHz). Due to different configurations of sensors, the operating frequencies and the measurement techniques involved with sensors might differ as well.

For the microwave sensor, the indirect method proposed is by using refractive index and relative complex permittivity. The microwave method is rather similar to the optical method in that it refers to the shifting in resonance or the change in reflection coefficient. The relationship between dielectric properties and moisture content can be expressed by a relative complex permittivity. The electric field distribution is influenced by the dielectric constant of the material, and this will affect the resonance frequency exhibited by the material as well. From this assessment, the author mentioned that the monopole type of microwave sensor is much more sensitive than many other types of slot sensors. However, the measurement precision is less due to its scattering and radiating tendency. In continuation of this research, the microstrip ring sensor for oil palm fruit measurement by Ahmad et al. (2019) [40] was proposed. This study was conducted in two parts, where the first measurement was for the fruit and the second

measurement was for the seed samples. From the study, the microstrip ring resonator is observed to be sensitive in monitoring the maturity of the palm fruit, but its precision of measurement is influenced by the size of the fruit it measures.

Pamornnak et al. (2013) [41] evaluate the oil palm fruit by measuring the dielectric constant at microwave frequency, that is to be exact, at 100 kHz. They used 20 fruit samples that consisted of four different ripeness groups. Each of the fruits was sliced into half and the flesh of the mesocarp was measured using the dielectric probe connected to the automatic network analyzer. The OER is observed to be inversely proportional to the dielectric constant. The researcher proposed using the spatial dielectric constant function. From the research, the spatial variation shows that the unripe has the highest ϵ' coefficient, whereas the fully ripe with an OER value of 55% has the lowest ϵ' coefficient, where the coefficients can be obtained using least square regression analysis to obtain the OER characteristic function. From all 28 samples tested, the results show 95.63% accuracy.

2.3.6. Inductive

Harun et al. proposed a new inductive concept based on a circular coil [7], a single flat-type air coil with various dimensions [5], dual resonance frequency effect [42] and the relative water content of oil palm FFB based on a single flat-type air coil estimated against week [43]. The Triple series flat-type air coil structure was also investigated with weekly field data analysis [44]. There are two structures tested for triple type structures: one with a fixed number of turns but a different length, and the other with a fixed length but a different number of turns. This inductive concept mainly uses the inductive-frequency (L_s-f) curve from the impedance analyzer as shown in Figure 2.9 to evaluate the fruit. The decrease in fruit capacitance as it ripens affects its resonance frequency. Hence, the performance of the triple series coil sensor shifted the resonance frequency lower compared to the single and dual coil sensors, and it

comparatively has a bigger difference between ripe and unripe. Hence, the performance of the first peak was highlighted in this study. In this study, the resonance frequency increases as the fruit ripens, but inversely proportional to the moisture content of the fruit. The total length of the triple air-coil with a constant number of turns allows more of the fruit's surface area to be in contact with the coil sensor and has less interwinding capacitance to take into account. Between two structured tests, the triple air coil sensor with the same number of turns but different lengths prove to show better results for this method.

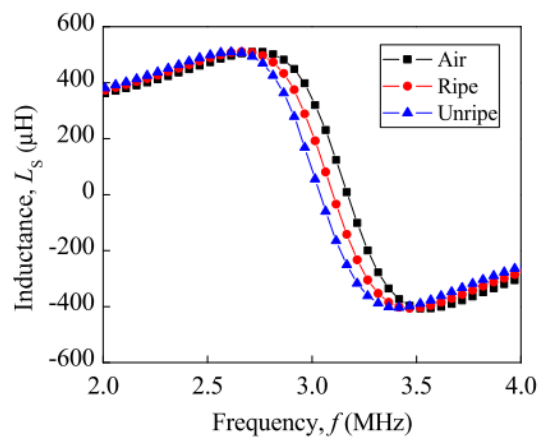


Figure 2.9: The oil palm fruit ripeness for L_s - f curve for single-flat type air coil for air, ripe, and unripe oil palm fruitlet [44]

Sinambela et al. (2020) [45] built a different inductive sensor structure that is composed of two stainless steel curved plates. Due to its different structure and frequency range used by the sensor, this sensor by the author [45] produces different results compared to Misron et al. (2017) [43]. This sensor operates at a low frequency (270–500 Hz), whereas Misron et al.'s (2017) experiment was conducted at a high frequency (8.5–9.5 MHz). The triple coil structure in series produces a lower first resonance frequency peak in comparison to the single coil, but it is still in a high frequency range (MHz). The experiment by Sinambela et al. (2020) [45] is to test this inductive sensor that consists of 600 fruits (100 ripe and 500 unripe) for the train and test data. From the data collected, a harvest time forecast was generated and a blind field test was conducted with 55 fruits. This sensor was tested with a 10–25-year-old oil palm fruit

tree where the oil palm bunches are quite high. This inductive sensor system architecture consists of discriminant analysis for ripeness identification and polynomial regression for harvest time prediction embedded in the system. The cross-validation confusion matrix for total ripe and unripe obtained was 92.5%. In this study, the researcher has proven that the inductive sensor system works well in field testing, with the accuracy of this system to determine oil palm ripeness being 100% for a blind test [45].

2.3.7. Capacitive

Aziz et al. (2011) [46] designed a capacitive sensing system to grade oil palm fruit FFB. In this method, oil palm FFB was placed between capacitive plates as a dielectric material, and the resulting capacitance voltage was measured. The relationship between the FFB ripeness index and its dielectric response was investigated at 100 kHz. The resultant capacitive response shows that it is sensitive to weight and also its maturity stages, as the capacitive response correlates linearly to bunch weight. The mature bunches were selected and the ripeness was assessed according to the oil palm fruit grading manual. Sinusoidal AC voltage was passed through the stainless steel conductive parallel plate, and the ripe and unripe FFB were placed between the two parallel plates. As the capacitance value changes, the voltage divider produces a different output. The unripe bunch shows an increase in the voltage due to the higher dielectric constant. The sensor response for the ripe bunch is lower compared to the unripe bunch of similar weight. This is due to the high dielectric value of the unripe bunch. The capacitive response is inversely proportional to the ripening of the fruit, but the weight of the fruit also contributes to the increase in the capacitance reading for this method.

The test frequency optimization for capacitive sensors was investigated by Abdul Aziz et al. (2020) [47]. The sinusoidal frequency input is between 20 kHz and 300 kHz. 60 oil palm fruitlets were collected. The frequency acts as a manipulative variable. The difference between

the peak-to-peak voltage value of the sensor response was constructed, and the data shows that it exhibits a negative linear relationship over the test frequency range of 20 kHz to 300 kHz. The ripe fruit has a higher impedance due to the low dielectric value, and the unripe fruit has a higher dielectric value, hence resulting in the low impedance. Small fruits are lighter and show a smaller reading compared to bigger fruitlets. The dielectric permittivity is highly influenced by the mass, hence affecting the density and the chemical composition as well.

2.3.8. Fruit battery

Minakata et al. (2018) [48,49] proposed a fruit battery method that utilizes the changes in fruit chemical composition. The fruit battery method consists of two electrodes that have different ionization tendencies, and the voltage difference between the ripe and unripe fruit was studied.

Misron et al. (2020) [50] propose continuation of the fruit battery approach by Minakata et al. but with a different implementation using the charging concept. From this study, they discovered that fruits with a moisture content of less than 44% have an average load voltage of between 20 and 30 mV, which are considered ripe fruits. The researcher [51] explored the concept further by implementing the concept with zinc and aluminum instead of the copper electrode used for previous research [50]. This paper also introduces different parameters in order to study the sensor sensitivity performance. The scholar concluded that the sensitivity of the fruit battery sensor increases when the parameters of the load resistance R_L , charging voltage V_C , and charging time increase.

Additionally, Misron et al. (2021) [52] present the implementation of the fruit battery method with four terminals with charging switches proceeding from the previous study. The study proceeds by using multiple terminals to evaluate the sensor's sensitivity by analyzing the relationship between the load voltage and the moisture content of the oil palm fruit. The sensitivity was improved when four terminals were used compared to single terminals. Hence,

it increases the accuracy of grading. The sample tested for this study consisted of 10 unripe, underripe, and ripe oil palm fruitlets were used. This sensor from this sensing category is invasive as the sensor electrode needs to be pricked into the fruit. This test can degrade and contaminate the tested sample fruitlet, hence the testing fruitlet on a bunch needs to be kept at a minimum and the extraction has to be done immediately after the test to prevent the deterioration of the fruit. Nevertheless, this research brings a new perspective on the method used for food quality parameters.

2.3.9. Electronic nose

An electronic nose has been used in the agriculture industry to evaluate the fruit quality by detecting the gas released by the fruit as it ripens. Shiddiq et al. (2021) [53] proposed and tested the application of an electronic nose to evaluate the ripeness of the oil palm fruit. The researcher tests an electronic nose system to characterize the ripeness level of oil palm fruit and its relationship with the hardness of the fruit measured with a penetrometer. The hardness of the fruit is measured by a penetrometer. This experiment uses nine oil palm FFBS with three different ripeness: unripe, ripe, and overripe. The system consists of a sensor and a sample chamber where the peeled fruit sample is inserted. The sensor chamber contains eight different MOS gas sensor modules with different gas identifiers. The output voltage of each sensor was measured, and the relationship between the fruit's hardness and oil palm fruit ripeness was investigated. The voltage output of the sensor is quantified using the integrated trapezoid area. The area of the trapezoid output voltage curve represents the response of the sensor to the fruit's ripeness category. The experiment conducted shows that MQ135 is the best gas sensor to detect the oil palm fruit ripeness stages. MQ135 detects benzene, alcohol, and ammonia concentrations in gaseous form. The research shows that as the fruit ripens, the rated voltage increases as it indicates that the volatile compound from the fruit in the form of palmitate acid and fatty acid increases.

2.3.10. Ultrasonic

Unlike all the other methods mentioned in this section, Suwannarat et al. (2012) [54] ultrasonic sensors are based on the fruit's mechanical properties, such as tactile features, to determine its ripeness. Basically, it is a tactile sensor that uses sound waves at a frequency that is higher than the human hearing limit that uses attenuation based on the ultrasonic transmission mode. The amplitude of the attenuation is controlled using a feedforward neural network (FNN). The ultrasonic parameter relates to the physiochemical and mechanical properties of the fruit. For this study, 36 fruits were collected and a 40 kHz ultrasonic transducer was connected to a digital oscilloscope to capture the waveform and transfer it to a PC, where the data was analyzed using MATLAB. The waveform is collected in the time domain obtained and for each fruit waveform, FFT data was collected. The system used is a mathematical model with back propagation. The attenuation parameter data is divided into training and test data. From the results obtained, the higher the oil content of the fruit, the higher the attenuation. This study also compares the method that was used previously in [55] with two-order polynomials, whereas this study uses FNN analysis.

2.5 Discussion

The literature comprises most of the non-computer vision methods in oil palm fruit maturity grading applications. It includes spectroscopy and non-spectroscopy methods. Optical spectroscopy, laser and Raman spectroscopy are categorized as spectroscopy methods. The non-spectroscopy methods mentioned in this review are thermal, microwave, inductive, capacitive, fruit battery, electronic nose, and ultrasonic.

The summaries of the methods applied to the spectroscopy method in order of appearance in this paper are presented in Table 2.3. The quality evaluation by the human grader is considered the "color" for the quality parameter evaluation.

Table 2.3: Summaries of method applied for oil palm FFB quality evaluation mentioned in the order of appearance in this section for spectroscopy method

Author	Method/device	Data/classification analysis	Quality Parameter
Hazir et al. (2012) [21,22]	Multiparameter fluorescent sensor	Classification and Regression Tree (C&RT)	Phenolic maturity content and color
Cherie et al. (2015a) [23]	Optical spectroscopy	Mean RGB histogram with Linear regression coefficient	Oil content
Cherie et al (2015b) [24]	Optical spectroscopy	Mean RGB and HSI data using multi-linear-perceptron artificial neural network (MLP-ANN)	Oil content
Albakri et al (2018) [25]	Diffuse reflectance spectroscopy	Reflectance characteristics	Color
Setiawan et al. (2019) [26]	Single wavelength light source and camera (680 nm)	Confusion matrix for image contrast and skewness	Color
Iqbal et al. (2019) [27]	Near Infrared Spectroscopy (NIR)	Partial Least Square (PLS) Regression	Moisture and oil content
Cherie et al. (2019) [28]	Reflectance shortwave infrared (SWIR)	Principal Component Analysis (PCA) and Partial Least Square (PLS)	Oil content, FFA, DOBI, carotene
Tuerxun et al. (2020) [29]	OPRID	Weka data mining tool and simple Lazy KStar algorithm validation	Color
Salambue et al. (2018) [30]	Biospeckle imaging using laser diode	Speckle modulation pattern	Color
Mohd Ali et al. (2020) [31]	Laser diode	Backscattering imaging and interaction	Oil content and color
Dan et al. (2018) [32]	Raman Spectroscopy	Peak intensity of particular wavenumber	Color
Nokkaew et al. (2019) [33]	Raman and Ft-NIR	Multiplicative scatter correction (MSC) and standard normal variate (SNV)	DOBI and carotenoids content
Raj et al. (2021) [34]	Raman Spectroscopy	K-nearest neighbor classifiers (KNN)	Color and phenolic content

The method mentioned in this paper includes both invasive and non-invasive techniques. Non-invasive techniques generally use cameras, such as thermal and spectroscopy methods that utilize the electromagnetic spectrum. Most of the other methods are rather invasive, such as fruit battery methods, as they require direct testing of the sample flesh itself. However, this will

not affect much of the fruit if it is done at the processing plant as the plant will undergo extraction immediately before the oxidation. It is noted that the fruit's oxidation will be triggered when its flesh is exposed to the environment. It is also important to know that the oil palm fruit is highly susceptible to mechanical damage. Any bruise that will boost the build-up of FFA in the fruit will jeopardize the quality of the oil palm fruit extracted.

Despite this paper's focus on the non-computer vision method, there are also combinations of methods with computer vision in order to increase the accuracy of the maturity grading, and it is proven to produce an increase in performance. Mohd Ali et al. (2020) [31] also use a combination of laser backscattering and computer vision, and the results show an average classification accuracy exceeding 85% with a good coefficient of determination for oil content and color values. Additionally, the use of an electronic nose is widely known to be used in combination with another sensor, such as an acoustic sensor for mango [56], a camera for banana [57] and NIR for peach [58]. Thus, it is interesting to observe the combination of one non-computer vision method with another to maximize its effectiveness in assessing the maturity of the oil palm fruits.

2.6 Summary

There are many different kinds of method used for oil palm FFB fruit maturity sensing application. This chapter aims to highlight various method by the researcher to evaluate the oil palm fruit ripeness evaluation. It is fascinating to discover researchers that take different approaches, for the same purpose. However, each sensor can be differing in the application stages of the sensing: pre-harvest and post-harvest.

CHAPTER 3

PREHARVEST EVALUATION

3.1 Overview

This chapter introduces the sensing method that uses a triple flat-type air coil structure to track the weekly progress of ripening on the oil palm tree. This evaluation is critical for the plantation worker to identify and distinguish the oil palm fruit ripening stages, as visual evaluation is insufficient to accurately determine the optimum oil palm FFB that can be harvested. The basic detection concept and the experimental methodology, the results and discussion of the results obtained and their relationship with the oil palm fruitlet's moisture content as well as the qualitative evaluation of its ripening condition are described in this chapter.

3.2 Methodology

An inductor is generally a passive element that stores energy in the form of a magnetic field. The basic detection concept in this study relies on the behavior of a non-ideal inductor at high frequency. In addition to the resistive component in a non-ideal inductor, there is a capacitive effect that affects an inductor's inductance property, as shown in Figure 3.1(a). Self-capacitance is significant at a high frequency that vastly depends on the coil's turn-to-turn effect. The presence of tiny capacitance between the windings is due to the coil's wire insulated coating and each winding section that has a different potential due to their own inductance and resistance. Figure 3.1(b) depicts the measurement graph, which includes an inductance-frequency ($Ls-f$) curve for air, ripe, and unripe fruit for a single flat-type air coil, similar to [23]. It is shown that unripe, ripe, and air follow the same sequence where unripe fruit has the lowest resonance frequency while air has the highest peak resonance frequency. As the fruit ripens,

the resonance curve increases and shifts towards the air's peak resonance frequency. Table 3.1 shows the impedance analyzer setup parameters that remained constant for the experiment conducted.

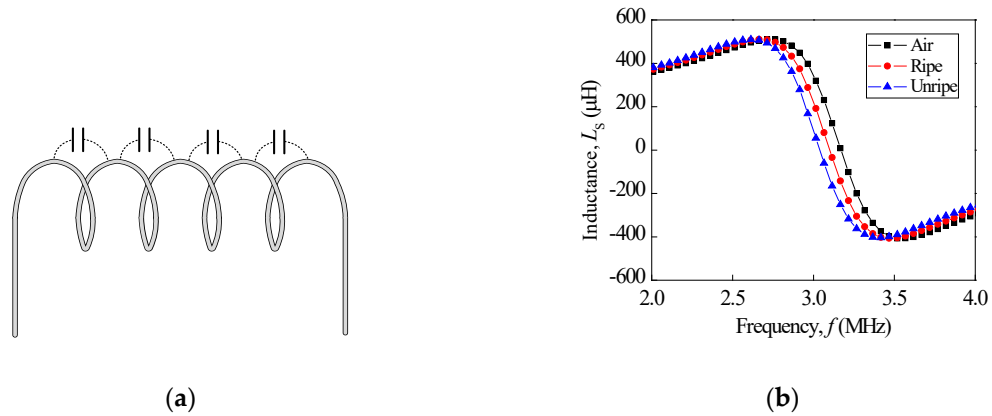


Figure 3.1: (a) Self-capacitance between coil turns and (b) oil palm fruit ripeness for L_s - f curve for single-flat type air coil for air, ripe and unripe

Table 3.1: Experiment setup parameters for triple flat-type air coil

Parameter	Type/Value
Measurement setup	Series (L_s - R_s)
Voltage	500 mV
Frequency range	20-10 MHz
Points	200
Coil wire diameter	0.12 mm

The experiment setup for triple flat-type air coil is shown in Figure 3.2(a). The triple coil sensor was directly connected to the impedance analyzer with the setup parameter presented in Table 3.1. The basic circuit representation for Figure 3.2(a) is as shown in Figure 3.2(b) where inductance (L_1 , L_2 and L_3), internal resistance (R_1 , R_2 and R_3), the total self-capacitance which composed of air (C_{a_1} , C_{a_2} and C_{a_3}) and fruitlet capacitance (C_{f_1} , C_{f_2} and C_{f_3}) in parallel. The dotted line indicates the assumed to be fruitlet capacitance that came from the oil palm fruitlet sample.

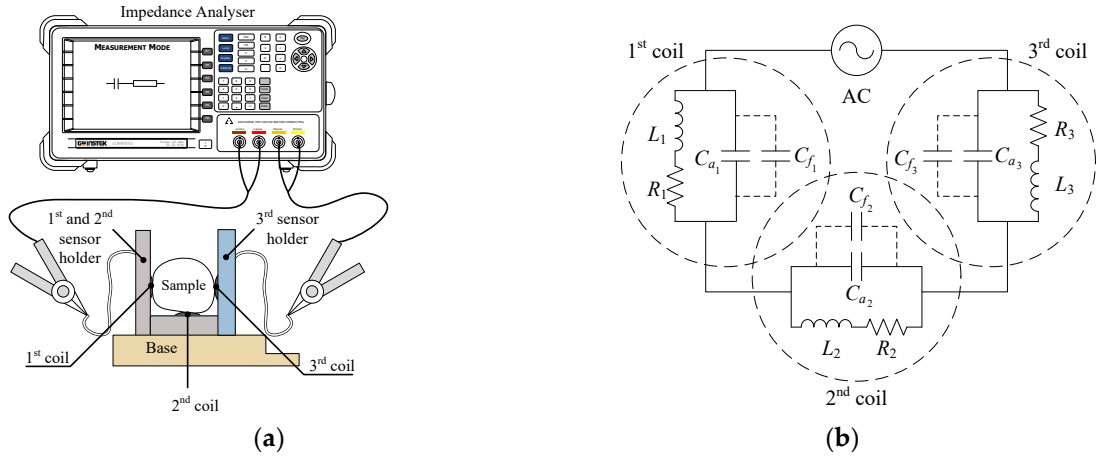


Figure 3.2: (a) Experiment setup for triple flat-type air coil sensor and its (b) equivalent circuit

Table 3.2 shows the coil configuration for two types of triple series flat-type air coil type I and II coil configuration used in this experiment. Triple I has constant number of turns $N=200$ and Triple II has constant length $l=5\text{mm}$. 1st, 2nd and 3rd coil configuration for both Triple I and II were arranged in series with increasing coil inductance magnitude where the 1st coil has the smallest inductance and the 3rd coil has the largest inductance.

Table 3.2: Type of coil configuration for triple series flat-type air coil sensor

Type	Constant parameter	1 st coil configuration	2 nd coil configuration	3 rd coil configuration
Triple I	$N=200$	$l=3\text{mm}$	$l=5\text{mm}$	$l=10\text{mm}$
Triple II	$l=5\text{mm}$	$N=140$	$N=200$	$N=400$

Figure 3.3(a) and 3.3(b) show the actual experiment setup without and with the sample. Weekly fruitlet samples were collected and measured using an impedance analyzer with a sample holder to hold the fruitlet sample in place. The coil sensor must be measured without any sample as a reference every week before the experiment, as shown in Figure 3.3(a), to eliminate errors caused by changing values of resonance frequency and maximum inductance over time. Figure 3.3(b) shows the fruitlet was sliced into three flat surfaces and the flesh touched the coil. This step is important to ensure that there must be no gap between the fruitlet flesh and the coil for maximum detection.

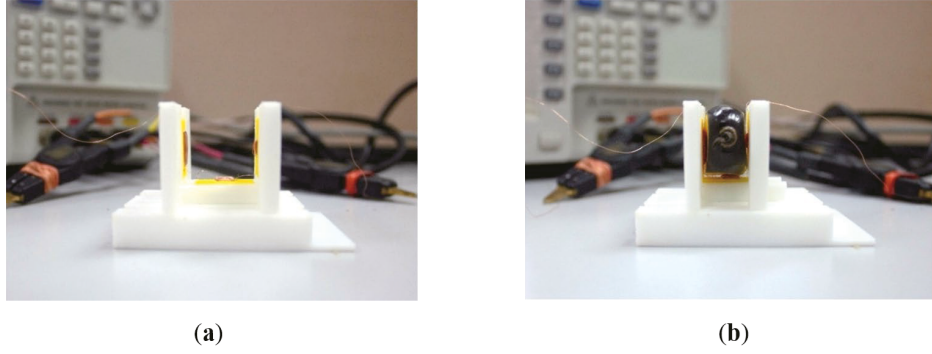


Figure 3.3: Triple flat-type air coil sensor (a) without and (b) with sample.

3.3 Experimental analysis

3.2.1 Self-capacitance and frutilet capacitance

The value of self-capacitance can be estimated by using the general resonance frequency formula as follows:

$$f_R = \frac{1}{2\pi\sqrt{LC}} \text{ (Hz)} \quad (3.1)$$

Where f_R (Hz) is the resonance frequency, L (H) is the inductance and C (F) is the capacitance. There are two different resonances principal present in this research: self-resonance frequency (SRF) and resonance frequency obtained through maximum peak in inductance-frequency ($L_s - f$) curve from impedance analyzer. Both resonances use the same formula as in Equation (1) but have different value of inductance L and frequency f_R . Figure 3.4(a) and 3.4(b) illustrate the differences between them. SRF is the resonance frequency that occurs at $L_s=0$ H and the standard value of inductance used is measured at 100 Hz [24]. On the other hand, resonance frequency is referred by the maximum inductance peak of the $L_s - f$ curve as shown in Figure 3.4(b). From this information, the self-capacitance can be estimated from both methods, but the approach used throughout this research is based on the information gained from Figure 3.4(b) as it is straightforward and simple.

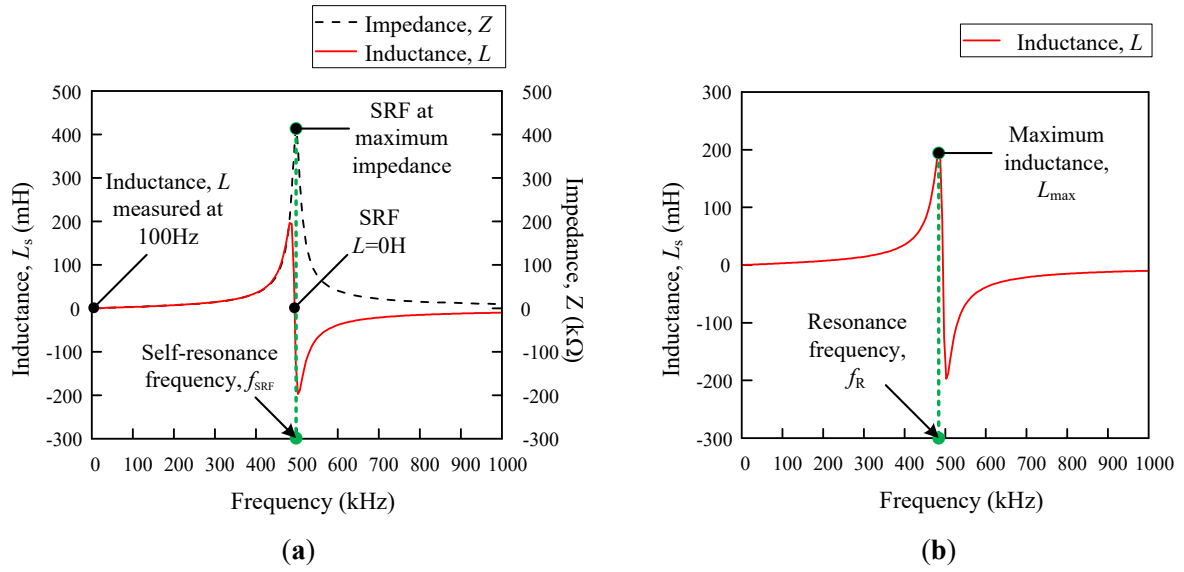


Figure 3.4: L_s – f curve illustrates (a) self-resonance frequency (SRF) and (b) resonance frequency.

Self-capacitance and fruitlet capacitance calculation are rather straightforward from Equation 1 and the parameter taken is as shown in Figure 3.4(b) and Equation 3.1 rearranged as:

$$C_R = \frac{1}{L_{max}} \cdot \frac{1}{(2\pi f_R)^2} \text{ (F)} \quad (3.2)$$

Where the C_R (F) is the calculated capacitance at resonance by substituting the maximum peak inductance, L_{max} (H) and the resonance frequency f_R (Hz) at L_{max} . The fruitlet capacitance C_f is determined from equation below:

$$C_f = C_R - C_a \text{ (F)} \quad (3.3)$$

Where C_f (F) is the fruitlet capacitance, C_R (F) is the total self-capacitance obtained through the Equation 3.2 and C_a (F) is the capacitance calculated using measured resonance frequency of air with no sample, consider measuring the air literally. Capacitance at peak resonance frequency C_R is introduced specially to avoid confusion with total self-capacitance that can be obtained at any given frequency using Equation 3.1.

3.2.2. Comparison analysis method

The sensor performance evaluation for flat-type air coil in this research involved several different parameters. First evaluation involved direct ripe-unripe comparison graph where the mean difference $\Delta\bar{f}_R$ (Hz) was calculated as follows:

$$\text{Error! Bookmark not defined. } \Delta\bar{f}_R = \bar{f}_{Rr} - \bar{f}_{Ru} \text{ [Hz]} \quad (3.4)$$

$\Delta\bar{f}_R$ (Hz) is the resonance frequency mean differences between mean ripe resonance frequency \bar{f}_{Rr} (Hz) and mean unripe resonance frequency \bar{f}_{Ru} (Hz). The approximation regression line fit follows general line equation below:

$$\text{Error! Bookmark not defined. } y = \alpha + \beta x \text{ where } \beta = \frac{\Delta y}{\Delta x} \quad (3.5)$$

Where y is the y -axis component and x are the x -axis component: week or moisture content according to the graph. The β magnitude value is the sensitivity of the coil sensor. The equation was further defined for resonance frequency against week as follows:

$$\text{Error! Bookmark not defined. } f_R = \alpha_{wf_R} + (\beta_{wf_R} \cdot w) \text{ (Hz)} \quad (3.6)$$

$$\beta_{wf_R} = \frac{\Delta f_{Rw}}{\Delta w} = \frac{\Delta f_{Rw}}{22} \text{ (Hz/week)} \quad (3.7)$$

$$\Delta f_{Rw} = \beta_{wf_R} \cdot 22 \text{ [Hz]} \quad (3.8)$$

Where f_R (Hz) is the resonance frequency, w is the number of week, α_{wf_R} (Hz) is the frequency at $w=0$ on resonance frequency against week graph which is an estimation for the unripe fruit, β_{wf_R} (Hz/week) is the sensitivity of the coil sensor resonance frequency with respect to week, Δf_{Rw} (Hz) is resonance frequency week difference and Δw is fixed at 22 weeks for Δf_{Rw} evaluation. For resonance frequency against moisture content graph line fit equations are:

$$\text{Error! Bookmark not defined. } f_R = \alpha_{mf_R} + (\beta_{mf_R} \cdot m_c) \text{ (Hz)} \quad (3.9)$$

$$\text{Error! Bookmark not defined. } \beta_{mf_R} = \frac{\Delta f_{Rm}}{\Delta m_c} = \frac{\Delta f_{Rm}}{100\%} \text{ (Hz/\%)} \quad (3.10)$$

$$\Delta f_{Rm} = \beta_{mf_R} \cdot 100\% \text{ (Hz)} \quad (3.11)$$

Where f_R (Hz) is the resonance frequency, m_c (%) is the moisture content in percentage value, α_{mf_R} (Hz) is the resonance frequency at $m_c = 0\%$ on resonance frequency against moisture graph which refers to assumed ripe resonance frequency, β_{mf_R} (Hz/%) is the sensitivity of the coil sensor with respect to moisture content, Δf_{Rm} (Hz) is resonance frequency moisture content difference and Δm_c (%) is fixed at 100% for Δf_{Rm} evaluation. Note that the resonance frequency against moisture content begin with 100% aims to follow the time vector (Week) pattern to observe its trend and therefore, its gradient value is a negative when compared to week.

Similarly, for fruitlet capacitance comparison, first evaluation involved direct ripe-unripe comparison graph where the mean difference $\Delta \overline{C_f}$ (F) was calculated as follows:

$$\text{Error! Bookmark not defined. } \Delta \overline{C_f} = \overline{C_{fr}} - \overline{C_{fu}} \text{ (F)} \quad (3.12)$$

$\Delta \overline{C_f}$ (F) is the fruitlet capacitance mean differences between mean ripe fruitlet capacitance $\overline{C_{fr}}$ (F) and mean unripe fruitlet capacitance $\overline{C_{fu}}$ (F). The linear line fit is the approximation regression line is the same as Equation 3.5 and the equation for fruitlet capacitance against week graph is as follows:

$$\text{Error! Bookmark not defined. } C_f = \alpha_{wC_f} + (\beta_{wC_f} \cdot w) \text{ (F)} \quad (3.13)$$

$$\text{Error! Bookmark not defined. } \beta_{wC_f} = \frac{\Delta C_{fw}}{\Delta w} = \frac{\Delta C_{fw}}{22} \text{ (F/week)} \quad (3.14)$$

$$\Delta C_{fw} = \beta_{wC_f} \cdot 22 \text{ (F)} \quad (3.15)$$

Where C_f (F) is the fruitlet capacitance, w is the number of week, α_{wC_f} (F) is the fruitlet capacitance at $w=0$ on fruitlet capacitance against week graph, β_{wC_f} (F/week) is the sensitivity

of the coil sensor of fruitlet capacitance with respect to week, ΔC_{f_w} (F) is fruitlet capacitance week difference and Δw is fixed at 22 weeks for ΔC_{f_w} evaluation. Fruitlet capacitance against moisture content line fit equations are as follows:

$$\text{Error! Bookmark not defined. } C_f = \alpha_{mC_f} + (\beta_{mC_f} \cdot m_c) \quad (\text{F}) \quad (3.16)$$

$$\text{Error! Bookmark not defined. } \beta_{mC_f} = \frac{\Delta C_{f_m}}{\Delta m_c} = \frac{\Delta C_{f_m}}{100} \quad (\text{F}/\%) \quad (3.17)$$

$$\Delta C_{f_m} = \beta_{mC_f} \cdot 100\% \quad (\text{F}) \quad (3.18)$$

Where C_f (F) is the resonance frequency, m_c (%) is the percentage of moisture content, α_{mC_f} (F) is the fruitlet capacitance at $m_c = 0\%$ on fruitlet capacitance against moisture graph, β_{mC_f} (F/%) is the sensitivity of the coil sensor with respect to moisture content, ΔC_{f_m} (Hz) is fruitlet capacitance moisture content difference and Δm_c is fixed at 100% for ΔC_{f_m} evaluation. The value of β_{mC_f} (F/%) for fruitlet capacitance against moisture content has positive gradient. This result is similar to result shown by K. Y. Lee et al. [18] where the dielectric constant increases with increasing moisture content.

Figure 3.5 summarizes the resonance frequency differences value obtained from each graph evaluated using Equation 3.4 for $\Delta \bar{f}_R$, Equation 3.8 for Δf_{R_m} and Equation 3.11 for Δf_{R_m} into a horizontal bar graph accompanied with their values. This allows the analysis to be assessed visually to observe the consistency of the differences for each coil. The same assessment was conducted for the fruitlet capacitance comparison with Equation 3.12 for $\Delta \bar{C}_f$, Equation 3.15 for ΔC_{f_w} , and Equation 3.18 for ΔC_{f_m} .

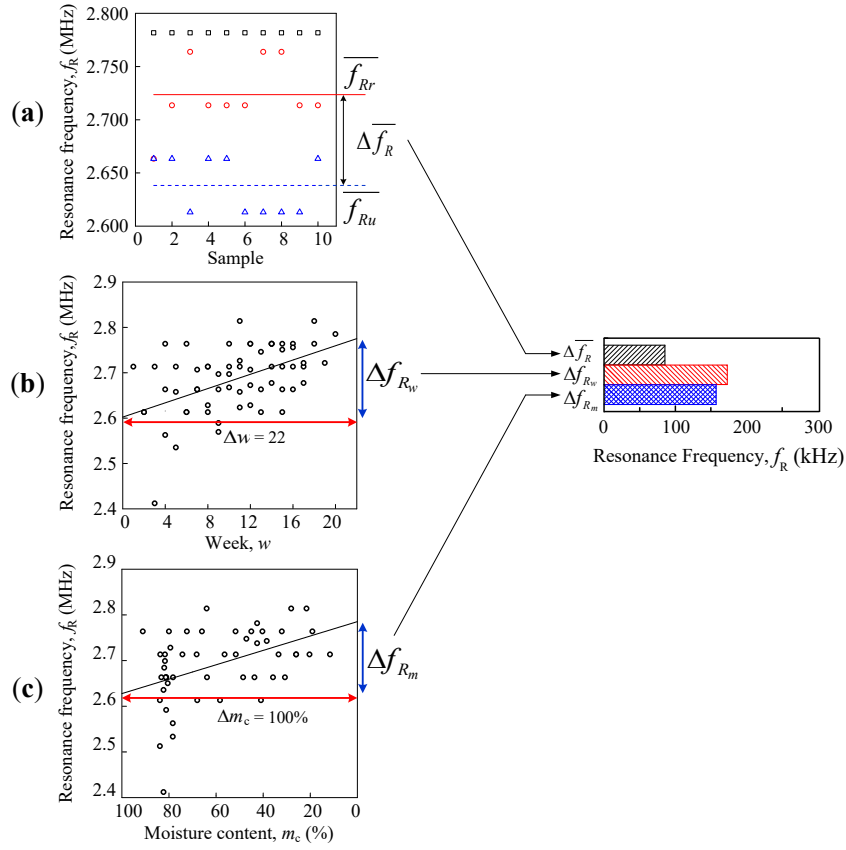


Figure 3.5: Resonance frequency for (a) direct ripe-unripe comparison, (b) resonance frequency against week and (c) resonance frequency against moisture comparison for selected flat-type air coil peak

Further analysis was conducted to the data in order to compare ripe-unripe, week and moisture differences. Simple statistical method was introduced to observe the variability and stability of the data. In order for the coil configuration to be selected, the coil needs to have small variability as well as high output sensitivity for best performance.

Differences mean $\bar{\Delta}$ and standard deviation σ were introduced as well as the coefficient of variation c_v to compare both triple flat-type air coil performance. Coefficient of variation c_v is a standardized measure of dispersion which is defined as the ratio of the standard deviation to mean. c_v is widely used to express precision and repeatability of the data [25].

$$\text{Error! Bookmark not defined. } c_v = \frac{\sigma}{\bar{\Delta}} \quad (3.19)$$

Where σ is standard deviation and $\bar{\Delta}$ is the average of the differences for resonance frequency and fruitlet capacitance as shown in Equation 3.20 and 3.21 respectively.

$$\text{Error! Bookmark not defined. } \bar{\Delta}f_R = \frac{\Delta\bar{f}_R + \Delta f_{Rw} + \Delta f_{Rm}}{3} \text{ (Hz)} \quad (3.20)$$

$$\bar{\Delta}C_f = \frac{\Delta\bar{C}_f + \Delta C_{fw} + \Delta C_{fm}}{3} \text{ (F)} \quad (3.21)$$

Where $\bar{\Delta}f_R$ (Hz) is resonance frequency differences mean which consist of $\Delta\bar{f}_R$, Δf_{Rw} and Δf_{Rm} from Equation 3.4, 3.8 and 3.11 respectively. Whereas $\bar{\Delta}C_f$ (F) is fruitlet capacitance differences mean that consist of $\Delta\bar{C}_f$, ΔC_{fw} and ΔC_{fm} from Equation 3.12, 3.15 and 3.18 respectively. For comparison between data sets with different means, the coefficient of variation is preferred instead of the standard deviation. Since the value of c_v is a dimensionless number independent of the unit in which the measurement is calculated, the sensor needed to be designed so that the coefficient of the variation c_v is close to zero where the data yields constant absolute error over the operational range.

3.4 Results and discussions

3.3.1. Bunch moisture content

The samples were taken weekly from the same selected bunch, and the sample fruitlets were measured with an impedance analyzer. After the measurement, the fruitlet moisture content was determined by using the oven-drying method. The sample was sliced and dried in the oven at $103 \text{ }^\circ\text{C} \pm 2^\circ\text{C}$ until the weight of the sample became constant. Based on the moisture content of the fruitlet, the fruitlet age is approximated as shown in Figure 3.6, where samples A, B, C, D, and E were assumed to be at Week 10, 1, 8, 2, and 4 respectively.

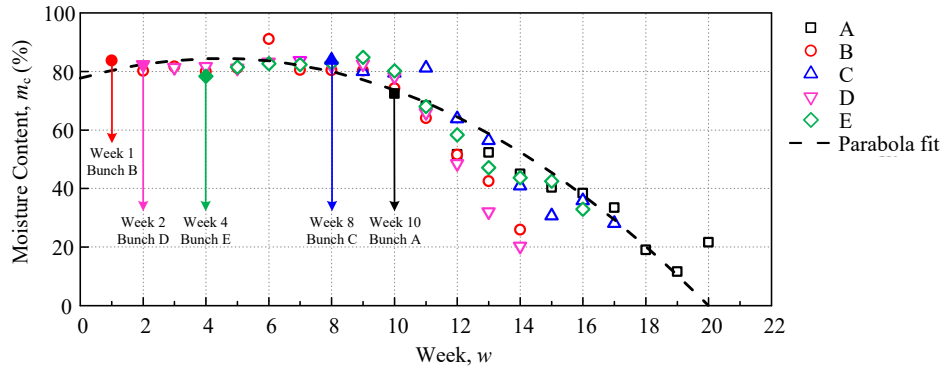


Figure 3.6: The moisture content for fruit sample bunch A, B, C, D and E.

The moisture content estimation equation is:

$$m_c = -3.348w^2 + 3.075w + 77.67, \text{ For } 0 < w < 20 \text{ [\%]} \quad (3.22)$$

Where $m_c(\%)$ is moisture content and w are number of weeks. The parabolic fit has coefficient of determination, $R^2 = 0.89367$, where the estimation is valid for the range begin at Week 1 that was deduced to be at 80.4% and Week 19 to be at 10.47%. Over-ripe fruit after Week 19 is predicted to be at a constant ripe percentage around 10% to 40% and does not go below 10%.

3.3.2. Inductance-Frequency Graph Characteristics

Figure 3.7(a) and 3.7(b) below shows the behavior of triple resonance of air, ripe, and unripe for Triple I and II that followed the sequence similar to its single flat-type air coil result in Figure 3.1b. Triple II was observed that has higher 1st maximum inductance peak when compared to Triple I. However, Triple II 2nd and 3rd peak were shorter compared to Triple I 2nd and 3rd peak. The 2nd and 3rd peak trend affects the peak detection and caused the data to be unstable. Therefore, the 1st peak performance is the important parameter in order to select the best performance indicator.

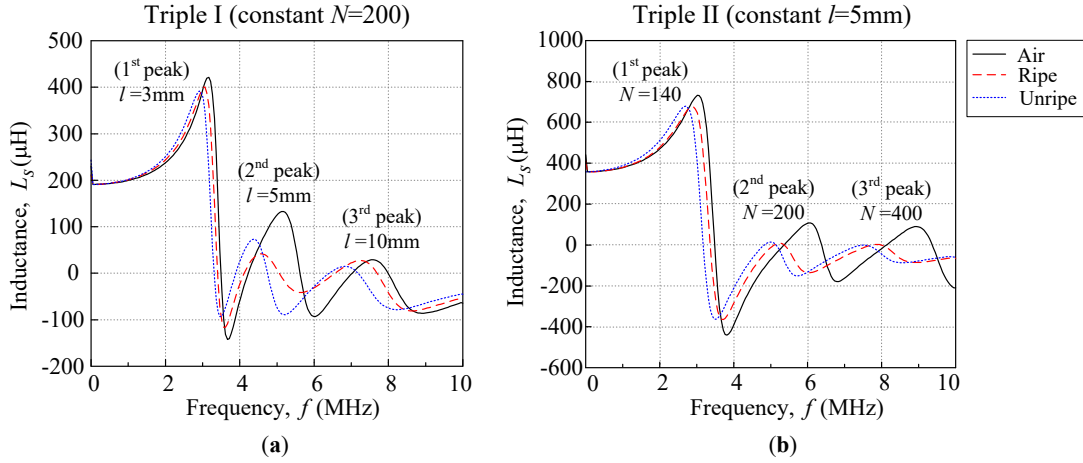


Figure 3.7: (a) Triple I and (b) Triple II L_s - f curves for air, ripe and unripe conditions

3.3.3. Peak resonance frequency, f_R

This section examines the peak resonance frequency differences between the ripe-unripe sample comparison, as well as week and moisture content evaluation of oil palm fruitlet sample for triple flat-type air coil.

Firstly, the ripe-unripe sample comparison is summarized in Table 3.3 and the mean value obtained from Figure 3.8(a) to 3.8(f) using Equation 3.4 for Triple I and II when calculating resonance frequency mean difference $\Delta \bar{f}_R$. Ripe-unripe comparison result shows that the difference between \bar{f}_{Rr} and \bar{f}_{Ru} decreases as the inductance of the coil increases, except for Triple II 2nd peak with small mean difference $\Delta \bar{f}_R = 5.03$ kHz. When comparing Triple I and II, it seems that Triple I has bigger $\Delta \bar{f}_R$ value for all peaks when compared to Triple II. Furthermore, even though the coil configuration for the 2nd peak is the same, the performance differs greatly as Triple I and Triple II $\Delta \bar{f}_R$ values are 256.28 kHz and 5.03 kHz respectively.

Table 3.3. Triple series coil mean resonance frequency for ripe and unripe with difference between them

Type	Peak	Ripe mean, $\overline{f_{RR}}$ (MHz)	Unripe mean, $\overline{f_{Ru}}$ (MHz)	Mean difference, $\Delta\overline{f_R}$ (kHz)
Triple I	1 st	2.980	2.849	130.66
	2 nd	4.437	4.181	256.28
	3 rd	6.915	6.643	271.35
Triple II	1 st	2.799	2.719	79.56
	2 nd	4.889	4.889	5.03
	3 rd	7.347	7.186	160.80

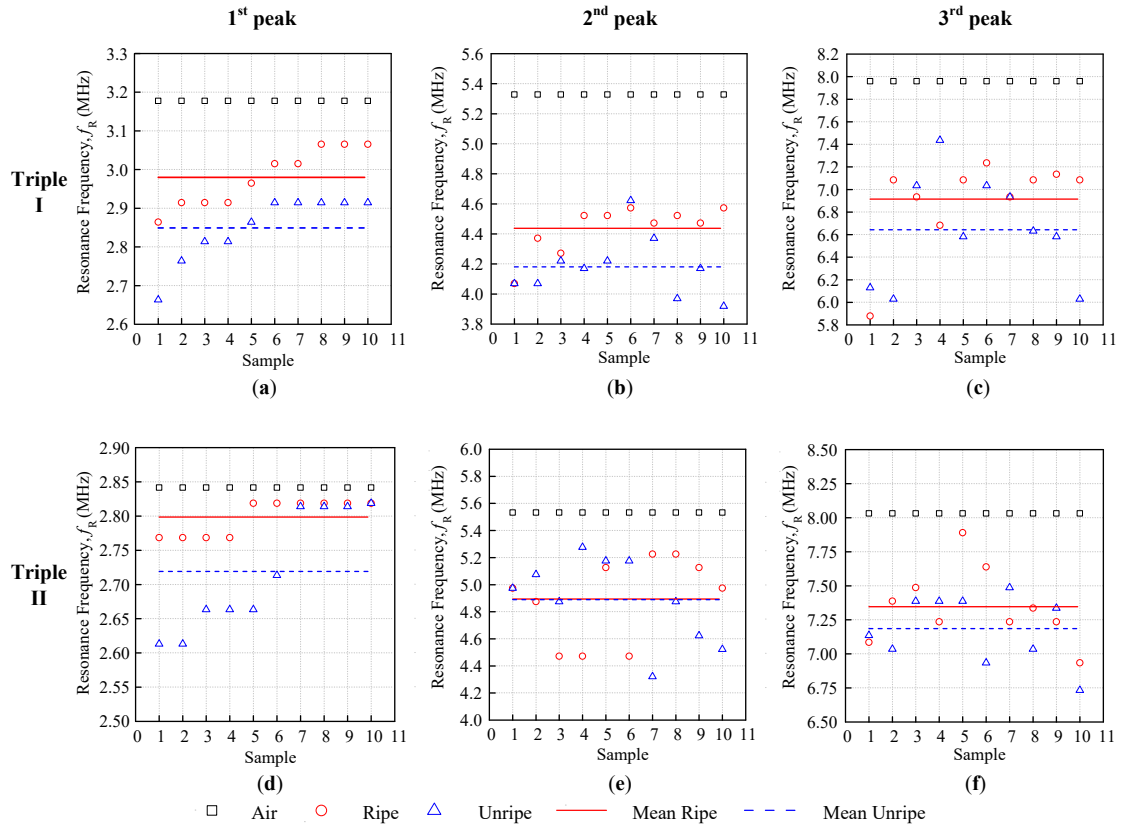


Figure 3.8: Ripe-unripe 1st, 2nd and 3rd peak resonance frequency comparison for Triple I (a)-(c) and Triple II (d)-(f)

Figure 3.9 and Figure 3.10 shows resonance frequency f_R against week and moisture content graph with line fit follows general approximate regression Equation (5). Triple I and II line fit obtained from Figure 3.8 for Triple I peaks and Figure 3.9 for Triple II peaks are summarized in Table 3.4. The linear regression equation for f_R against week is based on Equation (6) and for the linear regression equation f_R against moisture are based on Equation (9). The resonance

frequency against weeks shows all positive gradient β_{wf_R} , but moisture content of the fruitlet is inversely proportional to resonance frequency, therefore producing negative gradient β_{mf_R} . From Table 3.3, it is observed that Triple I sensitivity increasing with decreasing inductance for both against week and moisture content. Triple II f_R against week sensitivity β_{wf_R} is rather inconsistent, but for f_R against moisture sensitivity β_{mf_R} magnitude increase slightly with increasing coil inductance.

Table 3.4: Triple series coil $\alpha\beta$ value for resonance frequency against week and moisture graph

Type	Peak	Week		Moisture Content	
		α_{wf_R} (Hz)	β_{wf_R} (Hz/week)	α_{mf_R} (Hz)	β_{mf_R} (Hz/%)
Triple I	1 st	2.81×10^6	7.38×10^3	3.03×10^6	-2.14×10^3
	2 nd	4.43×10^6	11.90×10^3	4.75×10^6	-3.00×10^3
	3 rd	6.55×10^6	15.52×10^3	7.05×10^6	-5.26×10^3
Triple II	1 st	2.51×10^6	19.31×10^3	2.83×10^6	-1.75×10^3
	2 nd	4.91×10^6	6.20×10^3	5.09×10^6	-1.80×10^3
	3 rd	7.12×10^6	10.60×10^3	7.37×10^6	-2.16×10^3

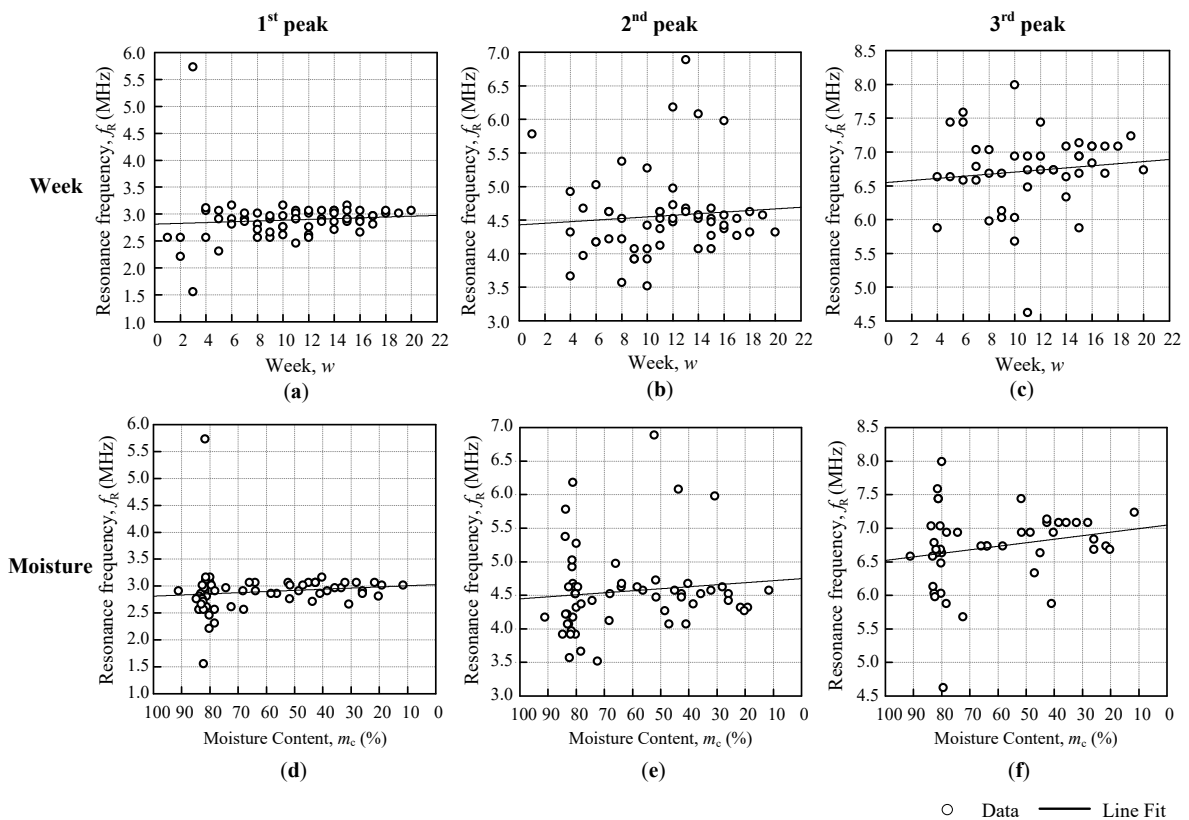


Figure 3.9: Triple I 1st, 2nd and 3rd peak resonance frequency against week (a)-(c) and moisture (d)-(f)

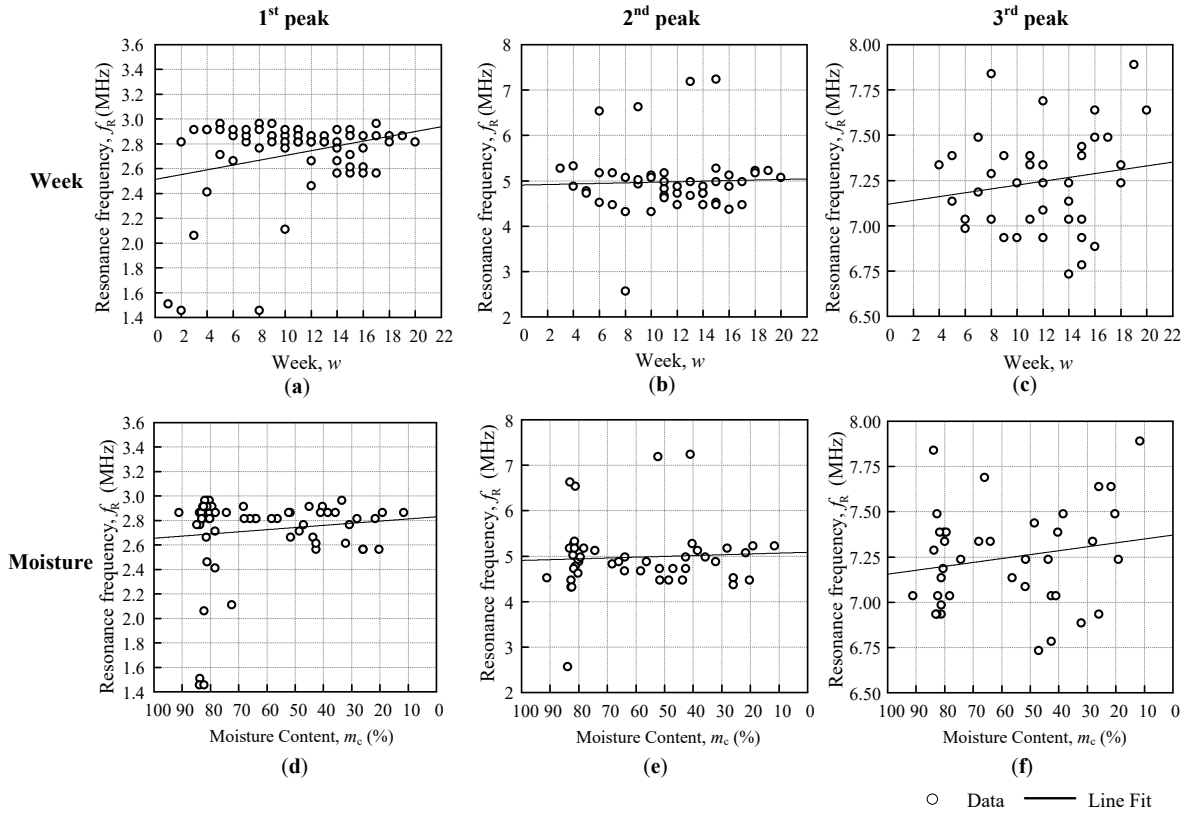


Figure 3.10: Triple II 1st, 2nd and 3rd peak resonance frequency against week (a)-(c) and moisture (d)-(f)

The resonance frequency evaluation comparison between peaks of Triple I and II are summarized in Figure 3.11. There are three parameters compared: $\Delta \bar{f}_R$, Δf_{R_w} and Δf_{R_m} . The linear regression equation for f_R against moisture are based on Equation 3.9 with the value of moisture Δf_R obtained through gradient β_{mf_R} by using Equations 3.10 and 3.11 with $\Delta m_c = 100\%$.

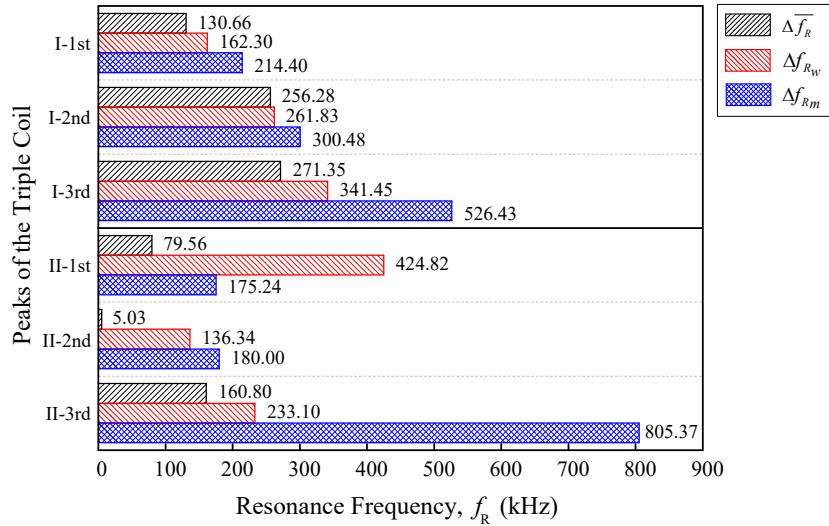


Figure 3.11: Triple I and II resonance frequency evaluation comparison for $\Delta \bar{f}_R$, Δf_{Rw} and Δf_{Rm}

Table 3.5 summarizes all the differences with differences mean, standard deviation and coefficient of variation c_v . When comparing the 1st peak of Triple I and II, the Triple I has smaller difference mean $\bar{\Delta f}_R=169.12$ kHz in comparison to Triple II $\bar{\Delta f}_R =226.54$ kHz. For 2nd peak, even though the coil configuration for both triple series is the same, it seems that Triple I has higher $\bar{\Delta f}_R$ as compared to Triple II by 165.74 kHz. The 3rd peak comparison shows that the Triple I has slightly lower than Triple II 3rd peak by 20.02 kHz. For coefficient of variation c_v with respect to difference mean and standard deviation, the peak comparison between Triple I and II shows that all c_v of Triple I is smaller than Triple II.

Table 3.5: Resonance frequency difference evaluation for triple series air coil

Type	Peak	Differences mean, $\bar{\Delta f}_R$ (kHz)	Standard deviation, σ_f (kHz)	Coefficient of variation, c_v
Triple I	1 st	169.12	42.28	0.2500
	2 nd	272.86	24.08	0.0882
	3 rd	379.74	131.78	0.3470
Triple II	1 st	226.54	178.26	0.7869
	2 nd	107.12	91.07	0.8501
	3 rd	399.76	353.13	0.8834

3.3.4. Fruitlet capacitance, C_f

This section studies the fruitlet capacitance differences between the ripe-unripe sample comparison, in addition to week and moisture content evaluation of oil palm fruitlet sample for triple flat-type air coil.

The fruitlet capacitance C_f is acquired when the self-capacitance of air coil C_a is deducted from self-capacitance of the coil with the fruitlet sample C_R , as expressed in Equation 3.3. In contrast to resonance frequency ripe $\overline{f_{Rr}}$ and unripe mean $\overline{f_{Ru}}$, mean unripe fruitlet capacitance $\overline{C_{fu}}$ is bigger than mean ripe $\overline{C_{fr}}$ as demonstrated in Figure 3.12. The fruitlet capacitance mean difference $\Delta \overline{C_f}$ is obtained through Equation 3.12 and tabulated in Table 3.5. Overall fruitlet capacitance mean ripe and unripe for Triple I is relatively higher than Triple II when compared peak-to-peak. The difference $\Delta \overline{C_f}$ for Triple I also higher than Triple II. But Triple I 2nd peak has shown incredibly big differences as compared to the rest of the peaks for both Triple I and II with $\Delta \overline{C_f} = 10.872$ pF. Even though Triple II has the same 2nd coil configuration with Triple I, but the value of $\overline{C_{fr}}$, $\overline{C_{fu}}$ and the difference $\Delta \overline{C_f}$ is not as high as in Triple I configuration.

Table 3.6: Triple coil mean fruitlet capacitance for ripe and unripe with difference between them

Type	Peak	Ripe mean, $\overline{C_{fr}}$ (pF)	Unripe mean, $\overline{C_{fu}}$ (pF)	Difference, $\Delta \overline{C_f}$ (pF)
Triple I	1 st	1.113	2.186	1.073
	2 nd	4.974	15.846	10.872
	3 rd	2.092	3.488	1.397
Triple II	1 st	0.147	0.395	0.247
	2 nd	1.471	2.032	0.561
	3 rd	0.356	0.452	0.095

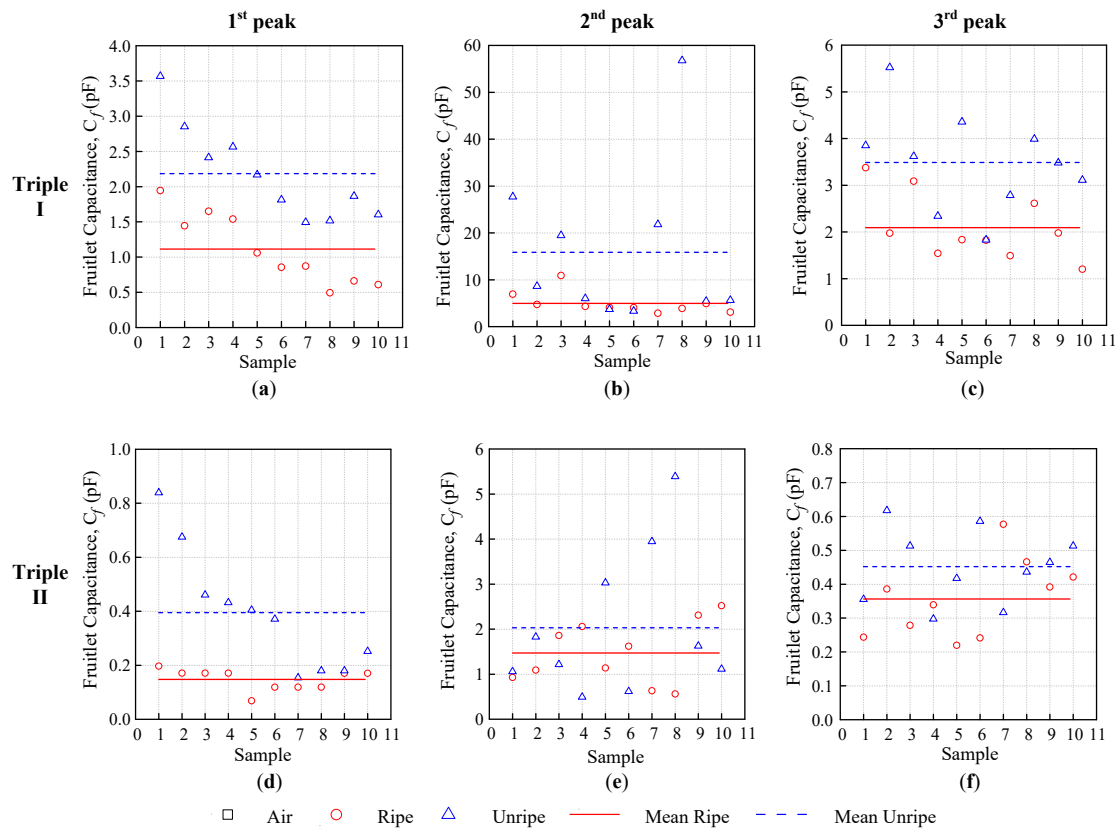


Figure 3.12: Ripe-unripe 1st, 2nd and 3rd fruitlet capacitance comparison for Triple I: (a)-(c) and Triple II: (d)-(f)

The individual fruitlet capacitance against week and moisture content graph is presented in Figure 3.12 for Triple I and Figure 3.13 for Triple II. The line fit equation parameter value from Figure 3.12 and Figure 3.10 are summarized in Table 3.7 below. Both figures are separated by the peaks: 1st, 2nd and 3rd with fruitlet capacitance against week and moisture. The linear regression equation is defined from Equation 3.13 and Equation 3.16 for both week and moisture graph. From Table 3.7, the α_{wC_f} value for the C_f against week shows an estimation for the unripe fruitlet capacitance, whereas α_{mC_f} value of the C_f against moisture content shows the fruitlet capacitance of air which the value observed is close to zero. The C_f against weeks gradient shows all negative β_{mC_f} , but C_f against moisture content shows positive gradient β_{mC_f} . It is because as the moisture content decreases, fruitlet capacitance decreases as well.

Table 3.7: Triple coil $\alpha\beta$ line fit value for fruitlet capacitance against week and moisture graph

Type	Peak	Week		Moisture Content	
		α_{wc_f} (F)	α_{wc_f} (F/week)	α_{mc_f} (F)	β_{mc_f} (F/%)
Triple I	1 st	4.272×10^{-12}	-193.301×10^{-15}	0.141×10^{-12}	32.314×10^{-15}
	2 nd	8.454×10^{-12}	-173.189×10^{-15}	2.647×10^{-12}	62.961×10^{-15}
	3 rd	4.606×10^{-12}	-139.312×10^{-15}	1.475×10^{-12}	25.313×10^{-15}
Triple II	1 st	0.814×10^{-12}	-25.878×10^{-15}	0.374×10^{-12}	2.666×10^{-15}
	2 nd	2.562×10^{-12}	-71.895×10^{-15}	0.622×10^{-12}	18.526×10^{-15}
	3 rd	1.878×10^{-12}	-13.404×10^{-15}	1.006×10^{-12}	11.739×10^{-15}

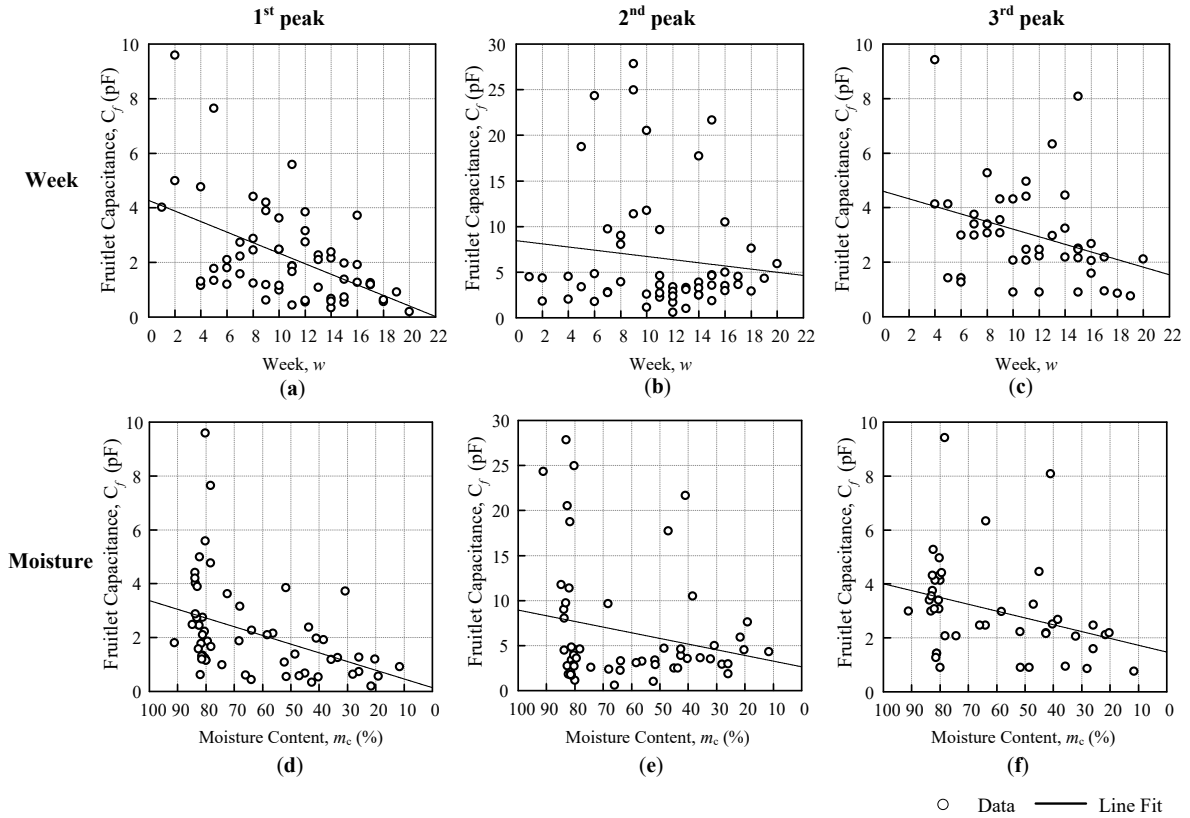


Figure 3.13: Triple I 1st, 2nd and 3rd fruitlet capacitance against week (a)-(c) and moisture content (d)-(f)

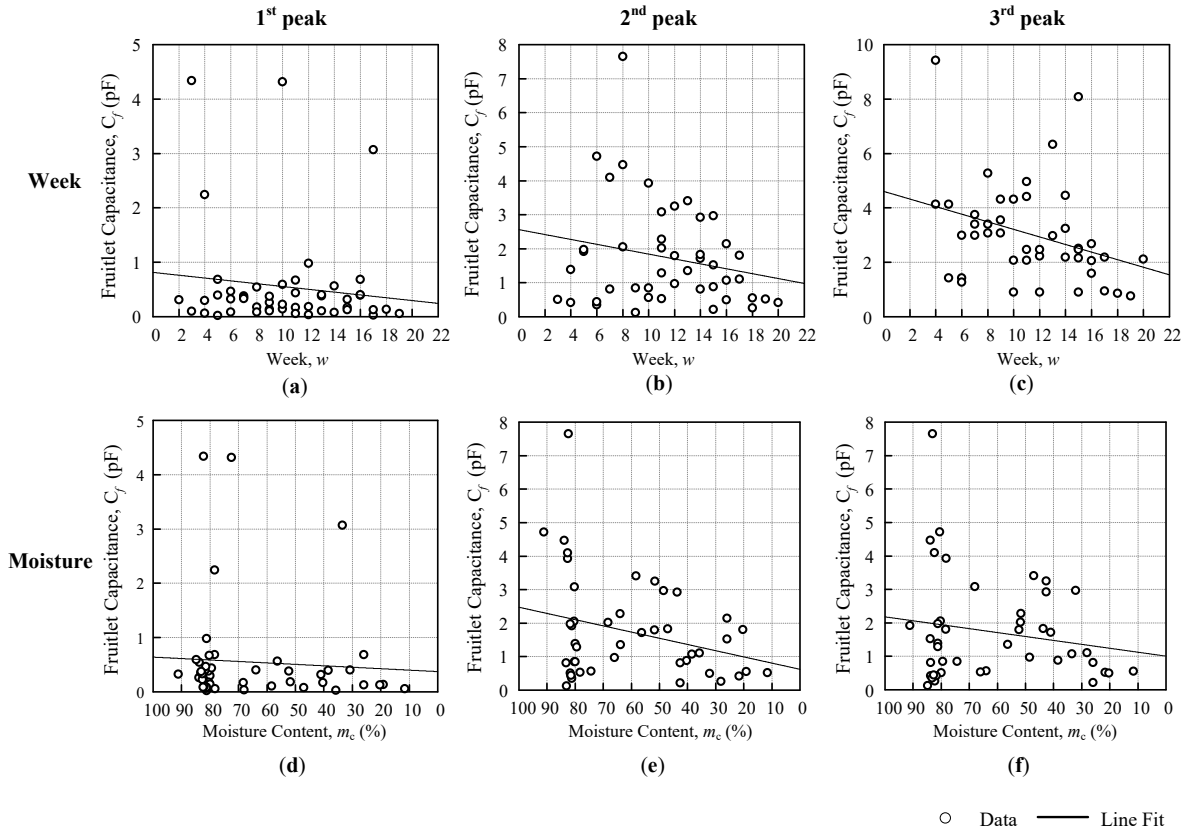


Figure 3.14. Triple II 1st, 2nd and 3rd fruitlet capacitance against week (a)-(c) and moisture (d)-(f)

Figure 3.15 summarizes the fruitlet capacitance comparison between peaks of Triple I and II. There are three parameters compared: $\Delta \overline{C_f}$ and ΔC_f for week and moisture. The fruitlet capacitance mean difference $\Delta \overline{C_f}$ is obtained through Equation 3.12 and tabulated in Table 3.5. Furthermore, for triple series comparison between peaks in Figure 3.11, Equation 3.15 with $\Delta w = 22$ are used to evaluate ΔC_{f_w} , whereas Equation 3.18 with $\Delta m_c = 100\%$ are used to evaluate ΔC_{f_m} .

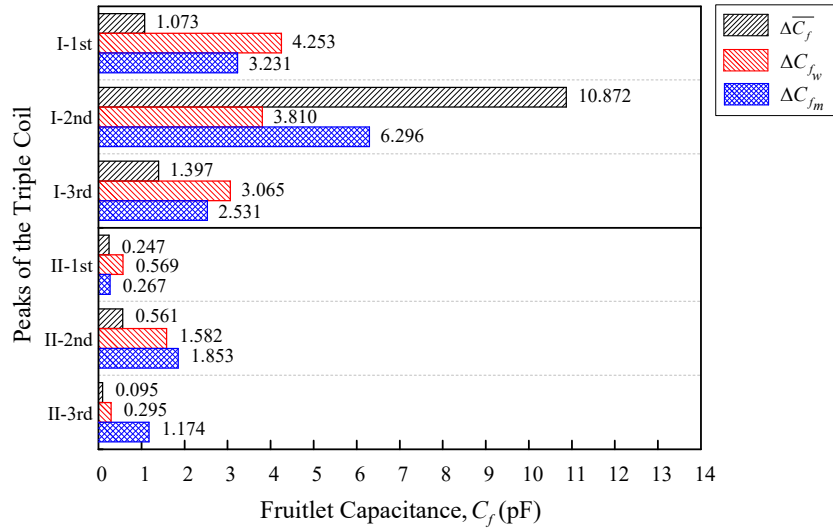


Figure 3.15: Triple I and II fruitlet capacitance evaluation comparison for $\Delta \bar{C}_f$, ΔC_{f_w} and ΔC_{f_m}

Table 3.8 summarizes all the differences from Figure 3.11 with differences mean, standard deviation and coefficient of variation c_v . Relatively, Triple I has higher fruitlet capacitance differences mean $\bar{\Delta C}_f$ as compared to Triple II. When comparing 2nd peak of both triple series, both performed with the highest $\bar{\Delta C}_f$ but Triple I 2nd peak is 5.25 times bigger as compared to Triple II 2nd peak even though both have the same with $N=200$, $l=5\text{mm}$ coil configuration. Moreover, the value of coefficient of variation c_v peak-to-peak comparison between Triple I and II peak shows that all c_v of Triple I are smaller than Triple II even though the 1st peak c_v for Triple II is smaller than Triple I, the 3rd peak of Triple II shows the worst c_v value with 1.1010. The high value of means indicates that the Triple II 3rd peak has inconsistent results for all tested evaluation ($\Delta \bar{C}_f$, ΔC_{f_w} and ΔC_{f_m}) with respect to its own difference mean and standard deviation ratio. From the results obtained, it is observed that Triple I shows the biggest fruitlet capacitance differences mean as compared to Triple II and has smaller average c_v for all peaks.

Table 3.8: Fruitlet capacitance difference evaluation for triple series air coil

Type	Peak	Differences mean, $\bar{\Delta}C_f$ (pF)	Standard deviation, σ_c (pF)	Coefficient of variation, c_v
Triple I	1 st	2.852	1.623	0.5692
	2 nd	6.993	3.582	0.5123
	3 rd	2.331	0.852	0.3654
Triple II	1 st	0.361	0.180	0.4998
	2 nd	1.332	0.681	0.5115
	3 rd	0.521	0.574	1.1010

3.4 Summary

For triple series flat-type air coil peak resonance frequency evaluation, Triple I and II were compared peak-to-peak for resonance frequency and fruitlet capacitance differences. When comparing the 1st peak of Triple I and II resonance frequency mean difference $\bar{\Delta}f_R$, the Triple I has smaller difference mean $\bar{\Delta}f_R=169.12$ kHz in comparison to Triple II $\bar{\Delta}f_R=226.54$ kHz. For coefficient of variation performance evaluation, Triple II peaks has a rather high c_v and therefore the level of dispersion around difference mean is high that shows that Triple II is less precise as compared to Triple I for resonance frequency difference comparison.

On the other hand, for fruitlet capacitance, Triple I has higher fruitlet capacitance differences mean $\bar{\Delta}C_f$ as compared to Triple II. When it comes to average coefficient of variation c_v , Triple I has a lower c_v value than Triple II, indicating that it is more precise since the lower coefficient of variation generates a more precise estimated range of data.

In short, Triple I with triple series coil with fix number of turns ($N=200$) shows better results when compare to Triple II coil with fix length ($l=5\text{mm}$). The total length with fix number of turns in Triple I series allow more fruit surface area touched the coil sensor and furthermore, it has less interwinding capacitance parameter intervention since it has same number of turns for all coil configuration in series.

Since this study also is a continuation from the previously studied novel inductive method, Table 3.9 below shows the comparison of triple series air coil with the previous version.

Table 3.9: Comparison between related research outcomes from previous study

Type of air coil	Structure parameter	Summary
Ring-type air coil [7]	$N = 5, 10, 15, 20$ $D_0 = 24\text{mm}, 26\text{mm}, 28\text{mm}$ $D_c: 0.25\text{mm}$	Resonant frequency decreases when the the air coil diameter increases. The resonant frequency decreases as the N decreases. The air gap that exist between the coil and the fruit sample cause data instability.
Single flat-type air coil [5]	$N = 60$ $l = 2\text{mm}, 3\text{mm}, 4\text{mm}, 5\text{mm}$ $D_c = 0.10\text{mm}, 0.12\text{mm}, 0.14\text{mm}, 0.16\text{mm}, 0.18\text{mm}$	Normalized resonant frequency of ripe samples, Nf_{tr} is higher than the normalized resonant frequency for unripe samples, Nf_{ru} . The value of the normalized resonant frequency, Nf_r decreases as the air coil's length increases. The difference between the ripe to unripe samples increases with the increasing air coil length. The flat surface of the air coil has overcome the air gap's existence in the ring type air coil. The structure of $l=5\text{mm}$ and $D_c=0.12\text{mm}$ shows the best performance that presents the highest percentage difference.
Dual flat-type air coil [42]	$N = 180-140, 200-140, 250-140$ $l = 5\text{mm}$ $D_c = 0.12\text{mm}$	Nf_{tr} leads the Nf_{ru} , same as previous result from single flat-type air coil. The dual flat type air coil analysis was conducted separately between peaks. The second peak has unstable inductance characteristics when compared to the first peak. The result shows improvement from the single coil ratio between ripe and unripe mean by 236% for 200-140 coil configuration.
Triple Flat-Type Air Coil [44]	Triple I (10-5-3mm) Fix $N=200$ Triple II (400-200-140) Fix $l=5\text{mm}$ $D_c = 0.12\text{mm}$	When averaging the 1 st peak and its equivalent single for 1 st peak from $\overline{\Delta f_R}$, Week Δf_R and Moisture Δf_R , the results showed that both Triple I and II has higher average than their equivalent single coil component.

SRF is reduced by connecting three flat-type air coils in a triple-type structure. This allows the use of the existing impedance analyzer. Unlike the impedance analyzer's general and expensive function, the device can be designed for a specific purpose. The sensor does not contain elaborate instruments like cameras; thus, it may be built cheaply. Since most of the world's oil palm plantations are in underdeveloped nations of the global south, this can reduce production costs.

CHAPTER 4

POSTHARVEST EVALUATION

4.1 Overview

The postharvest evaluation is personalized for the type of sensing device and the research objectives. The fruit battery method is quite destructive, and extraction must be completed immediately to avoid the accumulation of free fatty acids (FFA), which degrades the quality of the fruit oil extracted. This evaluation is proposed to be conducted at the mill, as harvesters may not consistently judge the ripeness of oil palm FFB across all plantations due to differences in height, lighting, and shadow. The chapter discusses sample preparation and how to determine the moisture content of a sample. The methodology for determining an appropriate load resistance value has been established, and the accuracy scores for fruit battery and computer vision are compared. Additionally, the chapter includes accuracy scores when the computer vision and fruit battery methods are combined.

4.2 Sample preparation and moisture content determination

The sample collection and experiment were conducted for three months from September 15th, 2017 to December 15th, 2017. The location where samples were obtained is at the Universiti Putra Malaysia oil palm plantation. Oil palm ripeness is determined by moisture content as shown in Table 4.1. From Table 4.1, when moisture content is 30% or less, it is labeled as "ripe". Meanwhile, moisture content between 30% and 53% is labeled "Under-ripe," and moisture content greater than 53% is labeled "Unripe". Table 4.1 is derived from the facts that FFB that has 30% moisture content has the maximum oil content [59] and FFB starts to mature when moisture content is estimated at 53%, as shown in Table 4.1 [43]. From Figure 4.1, oil

palm fruit mainly consists of moisture and lipids. The percentage of moisture and lipids in unripe fruit is 80.1% and 5.9%, respectively, while in ripe fruit it is 24.3% and 58.3%, respectively. It can be seen that the lipid content increases and the moisture content decreases as the fruit matures.

Table 4.1: Oil palm fruit ripeness based on moisture content

Ripeness category	Moisture content
Ripe	< 30%
Under-ripe	30% - 53%
Unripe	> 53%

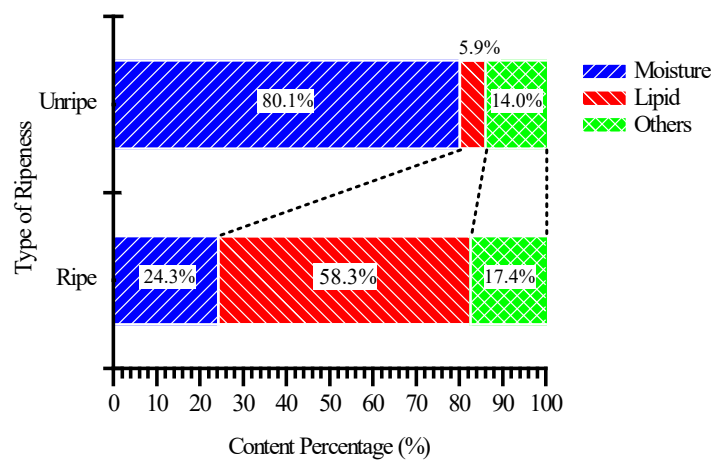


Figure 4.1: The composition of unripe and ripe fruit [43]

The oil palm fruit sample tested underwent moisture content determination measurement. The determination evaluation is performed on the day of sample collection after the measurements are taken. An infrared moisture meter (FD-610, Kett) is used to measure moisture content. The measurement heating temperature condition is 105°C with a drying time of 60 minutes.

4.3 Methodology

A total of 52 fruit samples were collected and used for this experiment. Among 52 fruit samples collected, 21 ripe, 15 under-ripe, and 16 unripe fruits were identified according to their moisture content from Table 4.1. All samples' photos are taken using an AR marker, then tested with the fruit battery method and, lastly, moisture content determination using an infrared moisture analyzer.

Firstly, the load resistance determination experiment uses only ripe and unripe fruits. 21 ripe and 16 unripe fruits are tested with load resistance ranging from 10 Ω to 1 M Ω . The reason is to get the differences between ripe and unripe samples to observe the best load resistance to be chosen for moisture content resolution analysis.

Moisture content resolution analysis uses all 52 fruits collected to identify the best load resistance that produces the highest sensitivity. The best load resistance results are used for accuracy score evaluation together with computer vision. The following subsections will elaborate further on computer vision and the fruit battery method applied in this study.

4.3.1. Basic concept of fruit battery method

This chapter proposed method to distinguish oil palm fruit ripeness by utilizing the principle of the fruit battery. Figure 4.2(a) shows a schematic diagram illustrating the principle of a fruit battery using an oil palm fruit. Equation 4.1 and 4.2 express the chemical equations of the fruit battery. A fruit battery basically generates an electromotive force when two electrodes having different standard electrode potentials are pierced through the fruit surface. Figure 4.2(a) shows that when a copper and a zinc electrode are pierced through the fruit, the zinc atom undergoes an oxidation reaction in which electrons are lost because zinc is higher in the electrochemical series than copper. The copper electrode accepts the electron from the zinc electrode, and the electron is combined with a positive hydrogen ion from the fruit, producing a hydrogen molecule. The movement of an electron generates current flow, thus producing electricity and behaving like a battery; hence it is called a fruit battery.



Figure 4.2(b) shows an equivalent circuit of a fruit battery. The equivalent circuit of the fruit battery can be expressed by an electromotive force V_i (V) and an internal resistance R_i (Ω).

Thus, the ripe and unripe oil palm fruit's internal resistance is high or low depending on the fruit's moisture content. The differences in internal resistance cause the load resistance voltage V_L (V) differences as shown in Equation 4.3. The fruit battery method aims to detect the difference in electrolyte load resistance voltage between unripe and ripe fruit.

$$V_L = \frac{R_L}{R_i + R_L} V_i \quad (4.3)$$

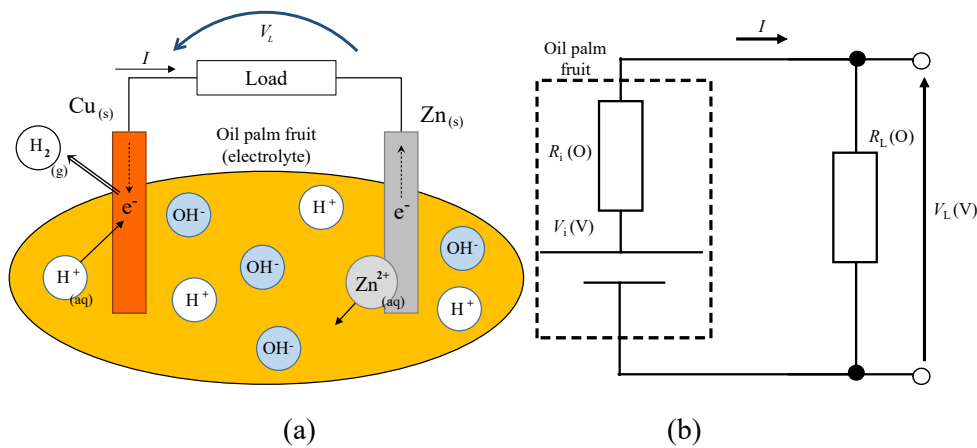


Figure 4.2: (a) Schematic diagram of fruit battery and (b) simple equivalent circuit of the fruit battery

4.3.2. Selecting load resistance value

Two experiments were conducted to determine a suitable load resistance for distinguishing oil palm ripeness stages for the fruit battery method. The first experiment aims to calculate the differences in the load resistance voltage. The load resistance voltage differences show the behavior of load resistance with oil palm fruit from different maturity stages with different moisture content. The second experiment aims to derive the resolution of the estimated moisture content for the field test. The resolution of the analog-to-digital (A/D) converter and the value of the slope of the regression formula between the load resistance voltage and moisture content are derived to determine the moisture content resolution.

4.3.3 The changing rate of the load resistance voltage

Figure 4.3 and Table 4.2 show the experimental setup schematic and experimental conditions, respectively. The load resistance voltage is measured using a digital multimeter (Pro's Kit, 3PK-600T) when electrodes are embedded into oil palm fruit as shown in Figure 4.3. Zinc and copper are used as the electrodes, and the dimensions of the electrodes are 16 mm long, 6 mm wide, and 0.5 mm thick. As determined from a previous study, the best distance between the electrodes is 2 mm with a 3 mm depth [49]. The total sample used is 37 fruits, where 21 and 16 fruits are identified as ripe and unripe fruit, respectively. In those conditions, the load resistance R_L (Ω) tested varied from 10 Ω to 1 M Ω .

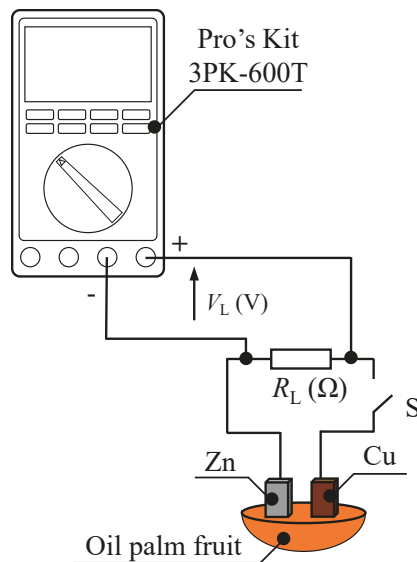


Figure 4.3: Fruit battery experimental setup

Table 4.2: Fruit battery experimental parameters

Item	Type/Value
Electrode material	Zinc, Copper
Electrode dimension	16 mm × 6 mm × 0.5 mm
Distance between electrodes	2 mm
Depth of electrodes	3 mm
Load resistance, R_L (Ω)	10, 100, 1k, 10k, 100k, 1M

In order to determine the value of load resistance that can effectively differentiate between unripe fruit and ripe fruit, the average load resistance voltage of both unripe and ripe fruit is

calculated. The average load resistance voltage is calculated in order to determine the value of the load resistance voltage that differentiates the value between an unripe and a ripe sample. Then, the load resistance voltage difference percentage of the load resistance voltage between unripe and ripe fruit is calculated using Equation 4.4.

$$|dV_L| = \left| \frac{V_{LRipe} - V_{LUripe}}{V_{LUripe}} \right| \times 100\% \text{ (V)} \quad (4.4)$$

dV_L is the load resistance voltage differences between unripe and ripe, V_{LRipe} is the ripe fruit's load resistance voltage, V_{LUripe} is the unripe fruit's load resistance voltage. Large $|dV_L|$, means larger resolution and this improves the load resistance sensitivity to distinguish the differences ripe and unripe fruits.

4.3.4 Resolution of estimated moisture content

To derive the resolution of the estimated moisture content, the slope value of the regression formula is determined using the least square method. A total of 52 oil palm fruit samples were used in this experiment. The best value of load resistance that was determined from previous experiments was selected for this experiment. Then a scatter plot between moisture content and the load resistance voltage is plotted and the regression formula between them is derived. Then the value obtained is compared to each other and evaluated. The load resistance voltage is measured three times, and the results are averaged.

4.3.5. Computer vision

For computer vision, a color chart and an oil palm fruit sample are taken together using a camera with a pixel resolution of 3264×2448 on a smartphone (iPhone 5S, Apple) as shown in Figure 4.4(a). At this time, the picture is taken under a fluorescent light and the color correction is conducted to decrease the influence of the variation of the photographing conditions by using the color chart [48]. The color chart with an AR marker is used to

automatically correct the color condition of images. Figure 4.4(b) shows the AR marker based on a color chart that has 16 color chips for color correction. The color chips are located around the marker, and each position of a color chip is automatically identified when the marker is detected. The proposed method requires a reference color chart image that is taken in the ideal lighting conditions. Target images for color correction are images that include target objects such as oil palm fruit and the AR color chart.

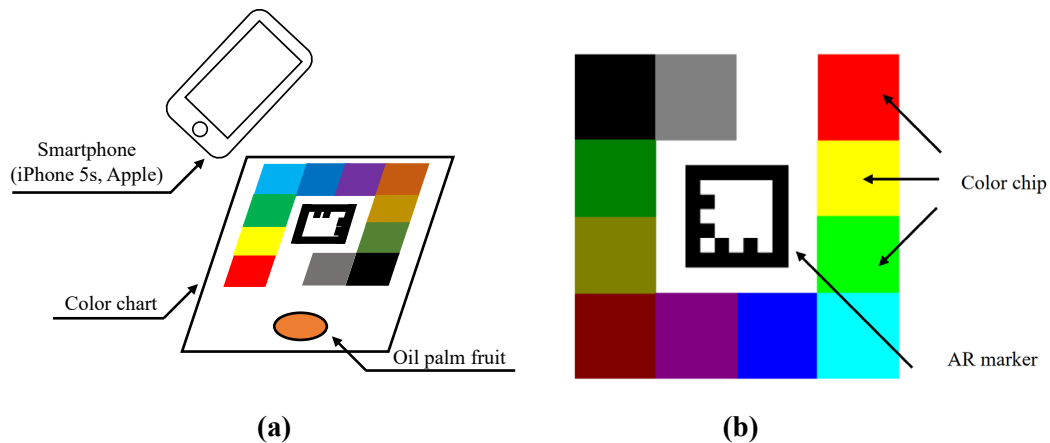


Figure 4.4: (a) Experimental setup of computer vision and (b) AR marker-based color chart for automatic color correction

In the correction process, a transformation matrix (regression coefficient matrix) in Equation 4.4 is calculated by linear multiple regression analysis as the pixel values of the color chips are closest when using 16 RGB values from the color chips on the reference image and the target image, respectively. The color of the target image is changed by multiplying the transformation matrix by the all-pixel matrix as shown in Equation 4.5. The advantage of the proposed color correction method is that it reduces the influence of environmental lighting and also makes the data acquisition procedure less complicated.

$$\begin{bmatrix} C'_R \\ C'_G \\ C'_B \end{bmatrix} = \begin{bmatrix} a_1 & a_4 & a_7 & a_{10} \\ a_2 & a_5 & a_8 & a_{11} \\ a_3 & a_6 & a_9 & a_{12} \end{bmatrix} \begin{bmatrix} C_R \\ C_G \\ C_B \\ 1 \end{bmatrix} \quad (4.5)$$

C' : a corrected pixel value
 C : an original pixel value
 a : a transformation matrix

After taking the picture, the average RGB value of oil palm fruit is extracted as shown in Figure 4.5. To extract the average RGB value, the picture taken is imported and the background is changed to black. In the background removal, a pixel value is set to 0 when the conditions (R-value > 90 and G-value > 90 and B-value > 90) are satisfied. Then, the average RGB value of the oil palm is calculated using Equation 4.6. The color feature R_{ave}/G_{ave} extraction is done by using Numpy, a numerical calculation library in Python.

$$Average\ pixel\ value = \frac{Total\ pixel\ value}{Total\ number\ of\ pixel} \quad (4.6)$$

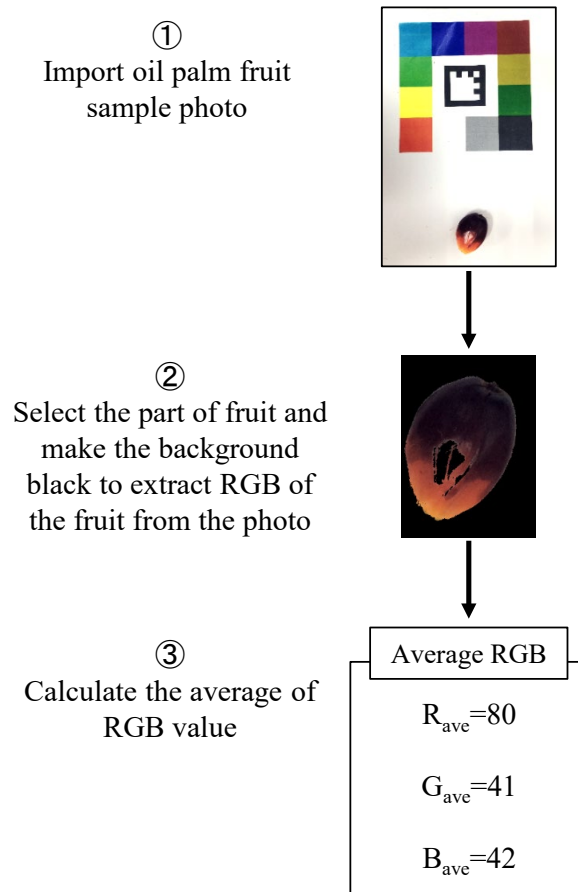


Figure 4.5: The flowchart of extracting color feature procedure

4.3.6 Accuracy scores

The accuracy score for three stages of ripeness is derived by a Support Vector Machine (SVM). An accuracy score is used as a metric to evaluate the classification model in this study. Table 4.3 shows the experimental conditions setup for SVM. From Table 4.3, the classification by SVM is performed with three features, that is: color, R_{ave}/G_{ave} ; fruit battery, V_L ; and combined computer vision with fruit battery method, V_L-R_{ave}/G_{ave} .

The hyperparameters for the grid search are $C = 1, 10, 100$, $\text{Gamma} = 1, 0.1, 0.01$, $\text{Kernel} = \text{Linear, rbf}$, and the number of divisions of k-fold cross validation is 8. Hence, the combination produces 18 sets of accuracy scores where each feature is compared for the best score. We used the ratio R/G because we set the reference wavelength to increase the stability. In the field of remote sensing and plant physiology, the ratio of light intensity wavelengths is often used to make vegetation indices such as Normalize Difference Vegetation Index (NDVI) [60] and the Green Normalize Difference Vegetation Index (GNDVI) [61].

Table 4.3: Classification condition setting for SVM

Item	Type/Value
Feature	Fruit battery: V_L Computer vision: R_{ave}/G_{ave} Combination: V_L-R_{ave}/G_{ave}
Score	Accuracy
Cost parameter	1, 10, 100
Gamma	1, 0.1, 0.01
Kernel	linear, rbf
Number of partitions of K-fold cross validation	8

4.4 Results and Discussions

4.4.1. The load resistance voltage differences

Figure 4.6(a) shows the average value of the load resistance voltage when it changes. As shown in Figure 4.6(a), there is a tendency for the unripe load resistance voltage to be greater than the ripe fruit in the 10Ω to $10 \text{ k}\Omega$, range. However, the difference between unripe and ripe does

not happen at 100 k Ω and 1 M Ω . Figure 4.6(a) also shows the load resistance voltage differences between unripe and ripe fruit.

According to Figure 4.6(b), 10 Ω is 76%, 100 Ω is 77%, 1 k Ω is 74%, and about 76% change of rate is obtained in the range of 10 Ω to 1 k Ω . For values larger than 1 k Ω , 10 k Ω is 57%, 100 k Ω is 27%, and 1 M Ω is 12%. When the load resistance increased, the change rate decreases. This is due to the load resistance voltage being the ratio of load resistance and internal resistance as mentioned in Equation 4.4. The oil palm ripeness evaluation is performed by measuring the difference between the internal resistance of unripe and ripe fruits. However, if the load resistance is too high compared to the internal resistance, the difference between the unripe and ripe fruit's internal resistance is too small to be detected.

From the results obtained in Figure 4.6(b), the changing rate of the load resistance voltage between unripe and ripe in the range of 10 Ω to 1 k Ω is the highest about 76%, compared to resistance value of 10 k Ω , 100 k Ω , and 1 M Ω tested. Hence, for the following section, the suitable load resistance is chosen from 10 Ω , 100 Ω , 1 k Ω by calculating the resolution of estimated moisture content.

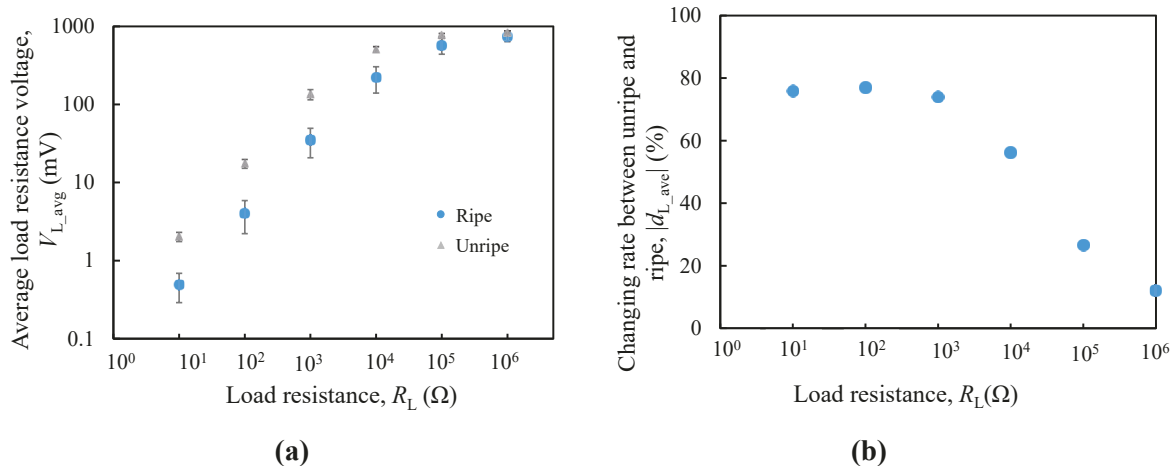
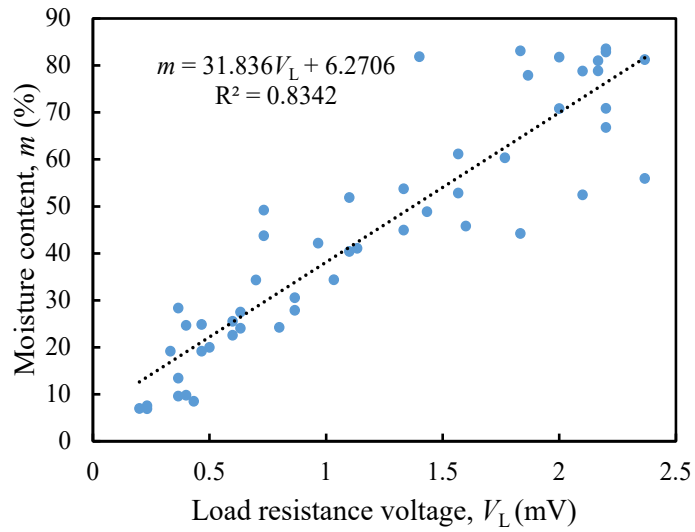


Figure 4.6: (a) The load resistance voltage of unripe and ripe as a function of load resistance and (b) the changing rate of load resistance voltage between unripe and ripe fruits

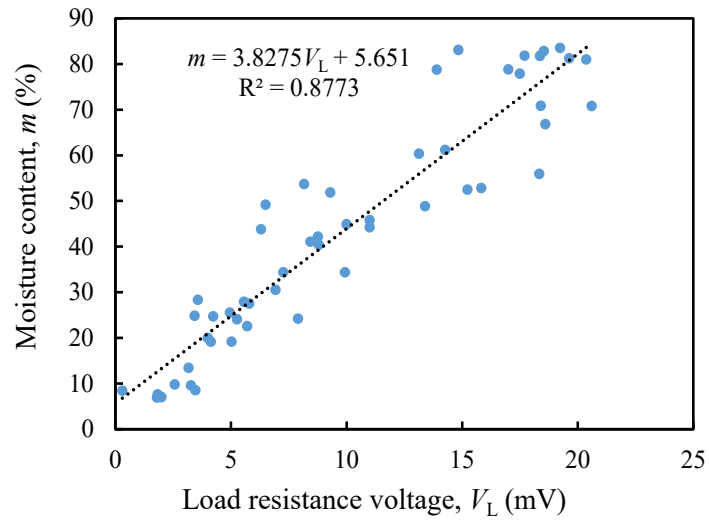
4.4.2. Resolution of estimated moisture content

Based on results from Figure 4.6(b), load resistance value of 10 Ω , 100 Ω and 1 k Ω are tested as shown in Figure 4.7. The moisture content varies directly with the load resistance voltage. As the oil palm fruit ripens, the load resistance voltage decreases. Figure 4.7 shows the prediction scatter plot together with its regression equation for each resistance value tested.

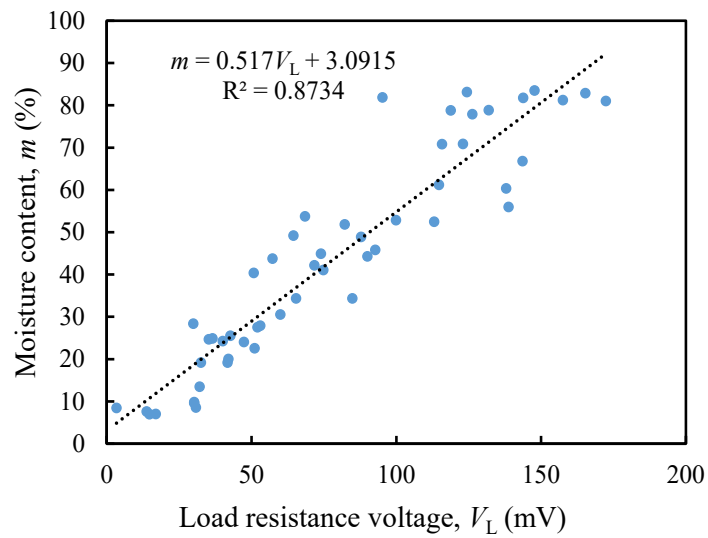
Higher resolution means that the device is sensitive enough to detect small change of the measurand in input. Thus, higher moisture content resolution with less than 1% can produce more accurate result with bigger sensitivity. From Figure 4.7, it is observed that 1 k Ω resistance gradient value is 0.517%/mV, whereas 10 Ω and 100 Ω have resolution of moisture content exceeds 1% with 31.8%/mV and 3.83%/mV respectively. Thus, 1 k Ω is the best load resistance value among them, as it has the highest moisture content resolution.



(a)



(b)



(c)

Figure 4.7. The prediction scatter plot between load resistance voltage and moisture content, (a) 10 Ω , (b) 100 Ω and (c) 1 k Ω

4.4.3. Comparison evaluation of fruit battery method and computer vision

Previous section results highlighted the emphasis on fruit battery evaluation and moisture content determination and getting the best resolution out of the load resistance tested. The best load resistance of 1 k Ω was selected to be used for comparison and combining features with the computer vision. The fruit battery load resistance voltage is measured with an electrode distance and depth of 2 mm and 3 mm, respectively, with the value of load resistance being 1 k Ω . For data evaluation, the average load resistance voltage of three measurements is used.

Table 4.4 shows the accuracy scores and standard deviation with their corresponding cost parameters, gamma and kernel, for the fruit battery method. The maximum accuracy score was 0.9038 (90.4%). However, there are three results with a 0.9038 accuracy score. The first results with a cost parameter of 1, gamma of 1, and a standard deviation of 0.0712 where the second set of results has the same standard deviation as the previously mentioned parameter, but with a cost parameter of 10 and gamma of 0.1. The third has a cost parameter of 100 and gamma of 1, but the standard deviation is 0.766. The best value among these three same accuracy scores is the standard deviation with the lowest value. Since low standard deviation means that the data is spread out closer to the mean [62].

Table 4.5 shows the SVM analysis results for computer vision method, where the highest accuracy score is 0.8654 (86.5%). This score has cost parameter = 1, gamma = 1, kernel = rbf with standard deviation = 0.0925.

Table 4.6 presents the results for fruit battery and computer vision combination accuracy score. The maximum accuracy score obtained for the combination scores is 0.9423 (94.2%) with cost parameter = 10, gamma = 0.1, and standard deviation = 0.0804.

Table 4.4: Accuracy score and standard deviation of each feature for fruit battery method

Cost parameter	Gamma	Kernel	Accuracy score	Standard deviation
1	1	linear	0.7308	0.1028
1	1	rbf	0.9038	0.0712
1	0.1	linear	0.7308	0.1028
1	0.1	rbf	0.6923	0.079
1	0.01	linear	0.7308	0.1028
1	0.01	rbf	0.6923	0.079
10	1	linear	0.8269	0.1471
10	1	rbf	0.8846	0.0648
10	0.1	linear	0.8269	0.1471
10	0.1	rbf	0.9038	0.0712
10	0.01	linear	0.8269	0.1471
10	0.01	rbf	0.6923	0.079
100	1	linear	0.8462	0.109
100	1	rbf	0.9038	0.0766
100	0.1	linear	0.8462	0.109
100	0.1	rbf	0.8846	0.0648
100	0.01	linear	0.8462	0.109
100	0.01	rbf	0.8077	0.1334

Table 4.5: Accuracy score and standard deviation of each feature for computer vision method

Cost parameter	Gamma	Kernel	Mean	Standard deviation
1	1	linear	0.6538	0.1042
1	1	rbf	0.8654	0.0925
1	0.1	linear	0.6538	0.1042
1	0.1	rbf	0.6538	0.1042
1	0.01	linear	0.6538	0.1042
1	0.01	rbf	0.6346	0.0959
10	1	linear	0.6538	0.1042
10	1	rbf	0.8269	0.1263
10	0.1	linear	0.6538	0.1042
10	0.1	rbf	0.6731	0.1413
10	0.01	linear	0.6538	0.1042
10	0.01	rbf	0.6538	0.1042
100	1	linear	0.6538	0.1042
100	1	rbf	0.8269	0.1263
100	0.1	linear	0.6538	0.1042
100	0.1	rbf	0.8269	0.1429
100	0.01	linear	0.6538	0.1042
100	0.01	rbf	0.6538	0.1042

Table 4.6: Accuracy score and standard deviation of each feature for combination of fruit battery and computer vision method

C	Gamma	Kernel	Mean	Standard deviation
1	1	linear	0.75	0.0959
1	1	rbf	0.9038	0.1204
1	0.1	linear	0.75	0.0959
1	0.1	rbf	0.75	0.0959
1	0.01	linear	0.75	0.0959
1	0.01	rbf	0.6923	0.0419
10	1	linear	0.8654	0.1266
10	1	rbf	0.8654	0.1289
10	0.1	linear	0.8654	0.1266
10	0.1	rbf	0.9423	0.0804
10	0.01	linear	0.8654	0.1266
10	0.01	rbf	0.6923	0.0419
100	1	linear	0.8846	0.0965
100	1	rbf	0.8462	0.1575
100	0.1	linear	0.8846	0.0965
100	0.1	rbf	0.9231	0.1101
100	0.01	linear	0.8846	0.0965
100	0.01	rbf	0.8654	0.1248

Table 4.7 shows the summary of maximum accuracy score and its standard deviation when each feature quantity is used: fruit battery, computer vision and combination. The accuracy score is 90.4% for the fruit battery method V_L , 86.5% for the color feature R_{ave}/G_{ave} , and 94.2% for the combined feature V_L-R_{ave}/G_{ave} . The standard deviation is 0.0712 for load resistance voltage, 0.0925 for color features, and 0.0804 for combined features. The combination of fruit battery method and computer vision to classify the oil palm fruit ripeness stage results shows accuracy score improvement. Computer vision method were tested on the same sample as the fruit battery method shows lower accuracy score compared to fruit battery method. On the other hand, by combining both features, the accuracy score increased to 94.2%.

The combination method proved to be helpful since the fruit battery method detects the change in fruit's chemistry and the computer vision using color feature detects the changes in color due to changing chlorophyll and anthocyanin content on the fruit's surface [22]. From this

study, the combined feature can classify the oil palm fruit maturity stages with higher accuracy compared to one-dimensional features.

Table 4.7: Maximum accuracy score and standard deviation of each feature

Feature	Accuracy (%)	Standard deviation
Fruit battery method using load resistance voltage, V_L	90.4	0.0712
Computer vision using color feature, R_{ave}/G_{ave}	86.5	0.0925
Combined feature (Fruit battery and computer vision), V_L-R_{ave}/G_{ave}	94.2	0.0804

Based on the results obtained from the experiments, a fruit battery prototype to test the oil palm fruit maturity was fabricated using open-source hardware Raspberry Pi 3 Model B as shown in Figure 4.8. 12-bit A/D converter is connected to Raspberry Pi 3 Model B with 0.8 mV A/D converter voltage resolution and 3.3 V drive voltage.

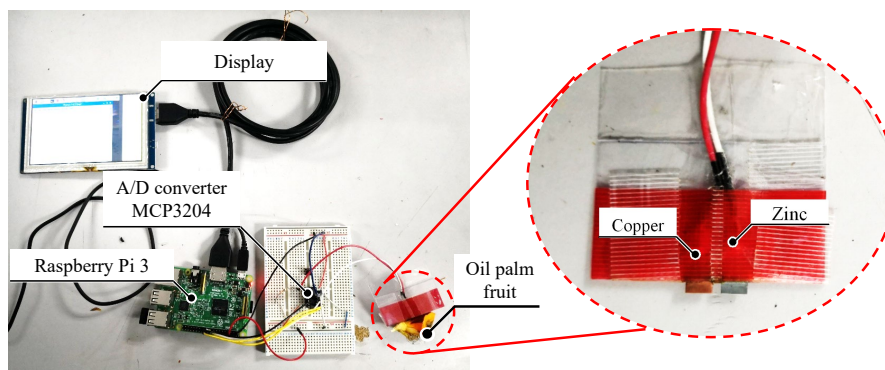


Figure 4.8: The prototype device that estimates oil palm fruit's moisture content using Raspberry Pi 3 Model B

4.5 Summary

This chapter studies the fruit battery load resistance determination that produces low resolution for high sensitivity results. As a result, the best load resistance obtained is 1 k Ω with a high changing rate between unripe and ripe fruit at 74% and moisture content resolution at 0.517%/mV. The accuracy score for fruit battery and computer vision is 90.4% and 86.5%, respectively. By combining the fruit battery and the computer vision method, the accuracy score calculated increased to 94.2%.

From this study, an automatic and low-cost color correction method is proposed by using augmented reality (AR) technology [63] and classifying them with a machine learning algorithm. The proposed method requires no strict calibration and adjustment at the measurement and automatically picks up the pixel values of a color chart with an AR marker based on the relative position of the marker. For current research, the accuracy scores obtained are saturated between 80% and 90%. This is due to FFB's surface color that exhibits similar color distinctiveness even though their ripeness stages are different. Therefore, in order to improve its accuracy, add-on feature color feature identification is proposed to be used simultaneously to increase the accuracy of classifying oil palm ripeness stages.

Both the fruit battery method and computer vision have advantages and disadvantages, but this study allows for the exploration of new fields of research that can be used in conjunction with the mill assessment. The advantage of this sensor is that it is cost-effective, and the sensor can be constructed cheaper and can be used to increase the accuracy of the oil palm FFB consignment evaluation sent to the mill for extraction. For future work, the number of samples needs to be larger for better sample population representation. Regardless, this study opens a new study for the oil palm fruit ripeness classification method.

CHAPTER 5

CONCLUSIONS

The preharvest evaluation is used to determine the optimal harvesting time, while the postharvest evaluation is used to evaluate the harvested FFB in order to categorize and classify it appropriately, as low-quality consignments can affect the oil extraction and oil quality of the OER.

For pre-harvest evaluation, the triple flat-type coil series configuration for the oil palm fruit maturity sensor was designed and fabricated. Furthermore, the relationship between oil palm fruitlet sample resonance frequency and fruitlet capacitance against week progression and moisture content was investigated. The triple flat-type air coil sensitivity and precision for oil palm fruit ripeness stage detection application were compared, and finally, the best triple series flat-type air coil was identified among the two types of coil series tested. Previous studies only focused on the effects of resonance frequency and did not take into account the maximum inductance nor examine the self-capacitance of the coil sensor. The importance of the basic concept of the coil's self-resonance frequency (SRF) in determining the resonance frequency of an inductor was also discussed. In the final evaluation, the performance of the first peak was highlighted in this study. The 2nd and 3rd peaks are extremely unstable and therefore make it very difficult to evaluate. Generally, resonance frequency increases with progressing ripening weeks but is inversely proportional to moisture content. However, fruitlet capacitance decreases with the progressing ripening weeks and is directly proportional to the moisture content percentage.

For postharvest evaluation, the thesis introduces the implementation of the fruit battery method. This evaluation investigates the low-resolution high sensitivity fruit battery load resistance determination. The best load resistance obtained is 1 k Ω with a 74 percent change rate between unripe and ripe fruit and a 0.517 percent moisture content resolution /mV. The accuracy score for fruit battery is 90.4 percent and for computer vision is 86.5 percent. The accuracy score increased to 94.2 percent by combining the fruit battery and computer vision. This study proposes an automatic and low-cost color correction method using AR and a machine learning algorithm. This method automatically picks up the pixel values of a color chart with an AR marker based on the relative position of the marker. Currently, the accuracy scores obtained are between 80% and 90%. This is because the surface color of FFB is similar even though their ripeness stages differ. Therefore, in order to improve classification accuracy of oil palm ripeness stages, color feature identification is proposed as an add-on feature. In addition to the mill assessment, this study allows for the exploration of new research fields that can be used in conjunction with the fruit battery method. This sensor has the advantage of being low-cost and can be used to improve the accuracy of the oil palm FFB consignment evaluation sent to the mill for extraction. In future research, more samples are needed to better represent the sample population.

There are many different kinds of method used as oil palm FFB fruit maturity sensing method, but the most common method is computer vision since it imitates the traditional evaluation that uses the color of the oil palm FFB as the indicator for its ripeness stages. This thesis highlights various method and attempt by the researcher to evaluate the oil palm fruit ripeness grading, such as optical spectroscopy, thermal, microwave sensor, inductive, fruit battery method and capacitive. It is interesting that researchers take different approaches, but aim for the same goal in determining the ripeness stage for oil palm FFB. By combining the few different method, the accuracy to determine the oil palm fruit ripeness stage can be improved.

Research related to the increase in yield and productivity in pre and postharvest stages is important as it can not only increase the production but also help the palm oil producer gain profit and minimize loss. The profit can in turn help the grower replant the oil palm tree sustainably, as the traditional slash-and-burn method that was used is cheaper but with terrible air quality and environmental consequences. Undeniably, oil palm has tremendous benefits and is the most productive crop, but its reputation is also tainted by its environmental consequences, such as deforestation. This thesis shows that most of the research came from the top oil palm producing countries, so there is hope for the prospect of a sustainable environment for humanity to thrive in the future.

REFERENCES

1. Chang, L.C.; Sani, a. R. a.; Basran, Z. An Economic Perspective of Oil Extraction Rate in the Oil Palm Industry of Malaysia. *Oil Palm Ind. Econ. J.* **2003**, *3*, 25–31.
2. Verheye, W. “Growth and production of oil palm.” Land use, land cover and soil sciences. *Encycl. Life Support Syst.* 2010, *2*, 1–32.
3. Hasibuan, H.A. Determination of Yield, Quality and Chemical Composition of Palm Oil and Palm Kernel Oil of Fresh Fruit Bunches with Variation Maturity as a Basic for Determining Harvest Maturity Standard. **2020**, *28*, 123–132.
4. (MPOB), M.P.O.B. *Oil Palm Fruit Grading Manual*; 2nd ed.; Malaysian Palm Oil Board (MPOB): Kajang, Selangor, 2003; ISBN 9679610918.
5. Misron, N.; Harun, N.H.; Lee, Y.K.; Sidek, R.M.; Aris, I.; Wakiwaka, H.; Tashiro, K. Improvement in sensitivity of an inductive oil palm fruit sensor. *Sensors (Switzerland)* **2014**, *14*, 2431–2448.
6. Ishida, M.; Abu Hassan, O. Utilization of oil palm frond as cattle feed. *JARQ, Japan Agric. Res. Q.* **1997**, *31*, 41–47.
7. Harun, N.H.; Misron, N.; Sidek, R.M.; Aris, I.; Ahmad, D.; Wakiwaka, H.; Tashiro, K. Investigations on a novel inductive concept frequency technique for the grading of oil palm fresh fruit bunches. *Sensors (Switzerland)* **2013**, *13*, 2254–2266.
8. Murphy, D.J. Oil palm: Future prospects for yield and quality improvements. *Lipid Technol.* **2009**, *21*, 257–260.
9. Tranbarger, T.J.; Dussert, S.; Joet, T.; Argout, X.; Summo, M.; Champion, A.; Cros, D.; Omoro, A.; Nouy, B.; Morcillo, F. Regulatory Mechanisms Underlying Oil Palm Fruit Mesocarp Maturation, Ripening, and Functional Specialization in Lipid and Carotenoid Metabolism. *Plant Physiol.* **2011**, *156*, 564–584.
10. Traveset, A.; Rodríguez-Pérez, J. Seed Dispersal. *Encycl. Ecol. Five-Volume Set* **2008**, 3188–3194.
11. Valenta, K.; Burke, R.J.; Styler, S.A.; Jackson, D.A.; Melin, A.D.; Lehman, S.M. Colour and odour drive fruit selection and seed dispersal by mouse lemurs. *Sci. Reports 2013 31* **2013**, *3*, 1–5.
12. Why does fruit change colour as it ripens? - BBC Science Focus Magazine Available online: <https://www.sciencefocus.com/nature/why-does-fruit-change-colour-as-it-ripens/> (accessed on Sep 17, 2021).
13. Utom, S.L.; Mohamad, E.J.; Ameran, H.L.M.; Kadir, H.A.; Muji, S.Z.M.; Rahim, R.A.; Puspanathan, J. Non-Destructive Oil Palm Fresh Fruit Bunch (FFB) grading technique using optical sensor. *Int. J. Integr. Eng.* **2018**, *10*, 35–39.
14. How can I find credible sources? - Paperpile Available online: <https://paperpile.com/g/find-credible-sources/> (accessed on Jan 4, 2022).
15. McLaughlin, R.P. Spectroscopy: Overview. *Encycl. Dairy Sci.* **2022**, 591–599.
16. de Broglie, L. *Research on the theory of quanta*; 1925; Vol. 10; ISBN 9781927763988.
17. Nanni, L.; Rigo, A.; Lumini, A.; Brahnam, S. Spectrogram Classification Using Dissimilarity Space. *Appl. Sci.* 2020, *Vol. 10*, Page 4176 **2020**, *10*, 4176.
18. Butler, L.R.P.; Laqua, K. Nomenclature, symbols, units and their usage in spectrochemical analysis-IX. Instrumentation for the spectral dispersion and isolation of optical radiation

- (IUPAC Recommendations 1995). *Pure Appl. Chem.* **1995**, *67*, 1725–1744.
19. Feng, Y.Z.; Sun, D.W. Application of Hyperspectral Imaging in Food Safety Inspection and Control: A Review. *Crit. Rev. Food Sci. Nutr.* **2012**, *52*, 1039–1058.
 20. Makky, M. Trend in non-destructive quality inspections for oil palm fresh fruits bunch in Indonesia. *Int. Food Res. J.* **2016**, *23*, S81–S90.
 21. Hazir, M.H.M.; Shariff, A.R.M.; Amiruddin, M.D.; Ramli, A.R.; Iqbal Saripan, M. Oil palm bunch ripeness classification using fluorescence technique. *J. Food Eng.* **2012**, *113*, 534–540.
 22. Hazir, M.H.M.; Shariff, A.R.M.; Amiruddin, M.D. Determination of oil palm fresh fruit bunch ripeness-Based on flavonoids and anthocyanin content. *Ind. Crops Prod.* **2012**, *36*, 466–475.
 23. Cherie, D.; Herodian, S.; Ahmad, U.; Mandang, T.; Makky, M. Optical characteristics of oil palm fresh fruits bunch (FFB) under three spectrum regions influence for harvest decision. *Int. J. Adv. Sci. Eng. Inf. Technol.* **2015**, *5*, 255–263.
 24. Cherie, D.; Herodian, S.; Mandang, T.; Ahmad, U. Advance models for camera-vision based oil content prediction of intact oil palm fruits (*Elaeis Guineensis* Jacq) on trees with nondestructive evaluation. *Int. J. Adv. Sci. Eng. Inf. Technol.* **2015**, *5*, 314–322.
 25. Albakri, N.; Abdullah, S.; Supian, L.S.; Arsad, N.; Zan, S.D.; Bakar, A.A.A. Assessment of Palm Oil Fruit Bunch Maturity based on Diffuse Reflectance Spectroscopy Technique. *2018 IEEE 7th Int. Conf. Photonics, ICP 2018* **2018**, 6–8.
 26. Setiawan, A.W.; Danudirdjo, D.; Ananda, A.R. Estimation of Nigrescens Palm Oil Ripeness using Contrast and Skewness from 680 nm Image. *Proc. - 2019 Int. Semin. Intell. Technol. Its Appl. ISITIA 2019* **2019**, 304–307.
 27. Iqbal, Z.; Herodian, S.; Widodo, S. Development of Partial Least Square (PLS) Prediction Model to Measure the Ripeness of Oil Palm Fresh Fruit Bunch (FFB) by Using NIR Spectroscopy. *IOP Conf. Ser. Earth Environ. Sci.* **2019**, 347.
 28. Cherie, D.; Rini, R.; Makky, M. Determination of the optimum harvest window and quality attributes of oil palm fresh fruit bunch using non-destructive shortwave infrared spectroscopy. *Proc. 2ND Int. Conf. Biosci. Med. Eng. Towar. Innov. Res. cross-disciplinary Collab.* **2019**, 2155, 020034.
 29. Tuerxun, A.; Mohamed Shariff, A.R.; Janius, R.; Abbas, Z.; Mahdiraji, G.A. Oil Palm Fresh Fruit Bunches Maturity Prediction by Using Optical Spectrometer. *IOP Conf. Ser. Earth Environ. Sci.* **2020**, 540.
 30. Salambue, R.; Adnan, A.; Shiddiq, M. Investigation of the ripeness of oil palm fresh fruit bunches using bio-speckle imaging. *J. Phys. Conf. Ser.* **2018**, 978.
 31. Mohd Ali, M.; Hashim, N.; Abdul Hamid, A.S. Combination of laser-light backscattering imaging and computer vision for rapid determination of oil palm fresh fruit bunches maturity. *Comput. Electron. Agric.* **2020**, *169*, 105235.
 32. Dan, S.A.M.; Hashim, F.H.; Raj, T.; Huddin, A.B.; Hussain, A. Classification of oil palm Fresh Fruit Bunches (FFB) using Raman spectroscopy. *Int. J. Eng. Technol.* **2018**, *7*, 184–188.
 33. Nokkaew, R. Determination of Carotenoids and Dobi Content in Crude Palm Oil By Spectroscopy Techniques: Comparison of Raman and Ft-Nir Spectroscopy. *Int. J. GEOMATE* **2019**, *16*, 92–98.
 34. Raj, T.; Hashim, F.H.; Huddin, A.B.; Hussain, A.; Ibrahim, M.F.; Abdul, P.M. Classification of oil palm fresh fruit maturity based on carotene content from Raman spectra. *Sci. Rep.* **2021**, *11*, 1–11.

35. Patkar, G.; Anjaneyulu, G.S.G.N.; Chandra Mouli, P.V.S.S.R. Palm fruit harvester algorithm for *elaeis guineensis* oil palm fruit grading using UML. In Proceedings of the 2015 IEEE International Conference on Computational Intelligence and Computing Research (ICCIC); 2015; pp. 1–6.
36. Zolfagharnassab S., V.C.N.; Mohamed Shariff A.R.; Ehsani R., J.H.Z.E.; I., A. Comparison of mean temperature taken between commercial and prototype thermal sensor in estimating mean temperature of oil palm fresh fruit bunches. *Int. Food Res. J.* **2016**, *23*, 91–95.
37. Makky, M.; Cherie, D. Pre-harvest oil palm FFB nondestructive evaluation technique using thermal-imaging device. *IOP Conf. Ser. Earth Environ. Sci.* **2021**, *757*, 012003.
38. Makky, M.; Cherie, D. Thermal and Optical Properties of Oil Palm FFB for Optimum Harvest Window Prediction. *IOP Conf. Ser. Earth Environ. Sci.* **2021**, *757*, 012004.
39. You, K.Y.; Wee, F.H.; Lee, Y.S.; Abbas, Z.; Lee, K.Y.; Cheng, E.M.; Khe, C.S.; Jamlos, M.F. A Review of Oil Palm Fruit Ripeness Monitoring Using Microwave Techniques in Malaysia. *IOP Conf. Ser. Mater. Sci. Eng.* **2020**, *767*, 012007.
40. Ahmad, A.F.; Abbas, Z.; Abrass, H.A.; You, K.Y. Optimum design of a microstrip ring resonator sensor to determine the moisture content in oil palm fruits and seeds. *BioResources* **2019**, *14*, 1819–1837.
41. Pamornnak, B.; Limsirorattana, S.; Chongcheawchamnan, M. Oil extraction rate determination technique based on dielectric constant of palm fruit. *Appl. Mech. Mater.* **2013**, *303–306*, 498–501.
42. Harun, N.H.; Misron, N.; Sidek, R.; Aris, I.; Wakiwaka, H.; Tashiro, K. Dual Resonant Frequencies Effects on an Induction-Based Oil Palm Fruit Sensor. *Sensors* **2014**, *14*, 21923–21940.
43. Misron, N.; Aliteh, N.A.N.A.; Harun, N.N.H.; Tashiro, K.; Sato, T.; Wakiwaka, H. Relative Estimation of Water Content for Flat-Type Inductive-Based Oil Palm Fruit Maturity Sensor. *Sensors (Switzerland)* **2017**, *17*, 10.
44. Aliteh, N.A.; Misron, N.; Aris, I.; Sidek, R.M.; Tashiro, K.; Wakiwaka, H. Triple Flat-Type Inductive-Based Oil Palm Fruit Maturity Sensor. *Sensors (Switzerland)* **2018**, *18*, 2496.
45. Sinambela, R.; Mandang, T.; Subrata, I.D.M.; Hermawan, W. Application of an inductive sensor system for identifying ripeness and forecasting harvest time of oil palm. *Sci. Hortic. (Amsterdam)*. **2020**, *265*, 109231.
46. Aziz, A.H.A.; Ismail, A.H.; Ahmad, R.B.; Isa, C.M.N.C.; Farook, R.S.M.; Husin, Z.; Ezanuddin, A.A.M.; Shakaff, A.Y.M. Design of a capacitive sensor for oil palm fresh fruit bunch maturity grading. In Proceedings of the 2014 2nd International Conference on Electronic Design, ICED 2014; Institute of Electrical and Electronics Engineers Inc., 2011; pp. 443–445.
47. Abdul Aziz, A.H.; Abuzar, S.A.; Azol, M.E.; Che Rose, N.H.; Mohmad, R.L. Test Frequency Optimization Using Single Factor ANOVA for Capacitive Oil Palm Fruit Ripeness Sensor. *IOP Conf. Ser. Mater. Sci. Eng.* **2020**, *932*.
48. Minakata, K.; Tashiro, K.; Wakiwaka, H.; Kobayashi, K.; Nagata, H.; Misron, N.; Aliteh, N. A.; Hasegawa, T.; Futamata, M. Preliminary study for discriminating oil palm ripeness by using color chart. In Proceedings of the The 32nd Annual Conference of the Japanese Society for Artificial Intelligence; Kagoshima City, Japan, 2018; pp. 8–11.
49. Minakata, K.; Tashiro, K.; Wakiwaka, H.; Kobayashi, K.; Misrom, N.; Aliteh, N.A.; Nagata, H. Proposal of Fruit Battery Method for Estimating Oil Palm Ripeness. *2018 12th Int. Conf. Sens. Technol.* **2018**, *399–402*.

50. Misron, N.; Azhar, N.S.K.; Hamidon, M.N.; Aris, I.; Tashiro, K.; Nagata, H. Fruit battery with charging concept for oil palm maturity sensor. *Sensors (Switzerland)* **2020**, *20*.
51. Misron, N.; Azhar, N.S.K.; Hamidon, M.N.; Aris, I.; Tashiro, K.; Nagata, H. Effect of charging parameter on fruit battery-based oil palm maturity sensor. *Micromachines* **2020**, *11*.
52. Misron, N.; Ibrahim, N.A.; Azhar, N.S.K.; Saini, L.M.; Vaithilingam, C.A.; Tashiro, K.; Nagata, H. Implementation of Four Terminal Fruit Battery with Charge Switching. *IEEE Access* **2021**, *9*, 1–1.
53. Shiddiq, M.; Sitohang, L.B.; Husein, I.R.; Ningsih, S.A.; Hermonica, S.; Fadillah, A. Hidung Elektronik Berbasis Sensor Gas Mos Untuk Karakterisasi Kematangan Buah Kelapa Sawit. *J. Tek. Pertan. Lampung (Journal Agric. Eng.* **2021**, *10*, 170.
54. Suwannarat, S.; Khaorapapong, T.; Chongcheawchamnan, M. Prediction of oil content in fresh palm fruit based on an ultrasonic technique. *Kasetsart J. - Nat. Sci.* **2012**, *46*, 318–324.
55. Suwannarat, S.; Khaorapapong, T.; Chongcheawchamnan, M. Predicting oil content of fresh palm fruit using transmission-mode ultrasonic technique. *World Acad. Sci. Eng. Technol.* **2011**, *81*, 859–862.
56. Zakaria, A.; Md Shakaff, A.Y.; Masnan, M.J.; Saad, F.S.A.; Adom, A.H.; Ahmad, M.N.; Jaafar, M.N.; Abdullah, A.H.; Kamarudin, L.M. Improved maturity and ripeness classifications of *Magnifera Indica* cv. harumanis mangoes through sensor fusion of an electronic nose and acoustic sensor. *Sensors (Switzerland)* **2012**, *12*, 6023–6048.
57. Chen, L.Y.; Wu, C.C.; Chou, T.I.; Chiu, S.W.; Tang, K.T. Development of a dual MOS electronic nose/camera system for improving fruit ripeness classification. *Sensors (Switzerland)* **2018**, *18*.
58. Huang, L.; Meng, L.; Zhu, N.; Wu, D. A primary study on forecasting the days before decay of peach fruit using near-infrared spectroscopy and electronic nose techniques. *Postharvest Biol. Technol.* **2017**, *133*, 104–112.
59. Siregar, I.M. Assessment of ripeness and crop quality control. In Proceedings of the The Malaysian International Agricultural Oil Palm Conference; Palm Oil Research Institute of Malaysia: Kuala Lumpur, Malaysia; pp. 740–754.
60. Jakubauskas, M.E.; Legates, D.R.; Kastens, J.H. Crop identification using harmonic analysis of time-series AVHRR NDVI data. *Comput. Electron. Agric.* **2003**, *37*, 127–139.
61. Moges, S.M.; Raun, W.R.; Mullen, R.W.; Freeman, K.W.; Johnson, G. V.; Solie, J.B.; Maru, S. Evaluation of green, red, and near infrared bands for predicting winter wheat biomass, nitrogen uptake, and final grain yield. *J. Plant Nutr.* **2005**, *27*, 1431–1441.
62. Field, A. *Discovering Statistics using IBM SPSS Statistics*; 5th ed.; Sage, 2018; ISBN 1446274586.
63. Kato, H.; Billinghurst, M. Marker tracking and HMD calibration for a video-based augmented reality conferencing system. *Proc. - 2nd IEEE ACM Int. Work. Augment. Reality, IWAR 1999* **1999**, 85–94.

Appendix

The comments from the thesis pre-defense

Title:

Title changes to be more specific. The previous title was too general (Prof Norhisam, Prof Sato)

→ The title changed from “Oil palm fruit maturity sensor” to “Oil palm fruit maturity evaluation with inductive coil and fruit battery method”.

Chapter 1:

- Motivation and thesis summary are unclear (Prof Tashiro)
- Recommendation for focus the motivation of Chapter 3 and 4 for preharvest and postharvest. (Prof Tashiro)
- Emphasis on importance of oil palm plantation management to introduce Chapter 3 and 4 motivation. (Prof Tashiro)
- Objective of the research in correspondence to chapter 2, 3 and 4. (Prof Tashiro)
- Introduce the importance of literature review in Chapter 2 (Prof Tashiro)
- What at the unresolved problems or issue (Prof Tashiro)
- Not enough background description and state the thesis contribution (Prof Sato)

Chapter 2:

- Data analysis comparison graph for clear view why the research is done and introduce why this method is proposed (Prof Norhisam)
- Add discussion and summary for the results of the literature review research (Prof Tashiro)
- Perspective of the maturity sensing trend in oil palm plantation (Prof Tashiro)
- Reason to why the survey is limited to 10 years. (Prof Sato)
- Conclusion for Chapter 2 that emphasis on the importance of this thesis (Prof Sato)

Chapter 3:

- Perspective practical use of the sensor mention in Chapter 3 (Prof Tashiro)
- The possibility of the Triple I sensor to help in oil palm plantation management in terms of practical use, performance and future issue for this sensor. (Prof. Tashiro)

Chapter 4:

- Elaboration needed – especially the raw data collection (Prof. Norhisam)

- Comparison with other sensor in Chapter 2, mention the advantage and disadvantage. (Prof Tashiro)
- Sensor that has the best performance and its qualitative comparison with “accuracy” (Prof. Tashiro)
- Relationship between sensor tested in Chapter 3 and 4 (Prof Sato)

Chapter 5:

- The coil sensor and nondestructive method evaluation are needed, future industrial application is expected (Prof Kobayashi)
- Discussion of cost in industrial application (Prof Kobayashi)